AN ABSTRACT OF THE THESIS OF

Mitchell A. Daniels for the degree of Honors Baccalaureate of Science in Mechanical Engineering presented on May 19, 2014. Title: Effects of Channel and Ratchet Geometry on Passive Pumping in an Open-ended channel Configuration

Abstract approved:

_____

Vinod Narayanan

Modern electronics have created increased demand for innovative cooling solutions. Typical forced convective cooling systems consist of pumps that circulate cooling fluid. However pumps can be unwieldy for many applications. This research is a continuation of work done at Oregon State University and Auburn University on the passive pumping of fluid in a preferential direction.

The geometry consisted of a channel with side walls comprised of 30-60 degree brass ratchets that were nominally 1 mm in pitch. Thin film heaters, located on the back side of the ratchets, were used to simulate the electronics heat source. The top and bottom sides of the channel were transparent to permit high speed visualization of boiling. A dielectric fluid, FC-72, was used as the working fluid. Several different geometries were considered including; different channel widths, asymmetric and symmetric surfaces, surfaces with flat sections, and half-pitch offset. Runs with similar conditions were chosen to compare the effect of the geometric changes on preferential bubble motion. Image processing was used to retrieve the velocity of the bubbles in the channel and the number of venting events to classify the performance.

The vapor bubbles exhibited a preferential direction in the direction of the ratchet with the lower angle. Bubble velocities up to 160 mm/s were observed during the tests. Symmetric ratchets and flat surfaces were observed to have no preferential direction.

Key Words: Heat Transfer, Electronics Cooling, Boiling, Microstructures

Corresponding e-mail address: danielmi@onid.oregonstate.edu.com

Effects of Channel and Ratchet Geometry on Passive Pumping in an Open-ended channel Configuration

By

Mitchell A. Daniels

A PROJECT

Submitted to

Oregon State University

University Honors College

In partial fulfillment of
the requirements for the
degree of
Honors Baccalaureate of Science in Mechanical Engineering (Honors Scholar)

Presented May 19, 2014
Commencement June 2014

Honors Baccalaureate of Science in Mechanical Engineering project of Mitchell A. Daniels presented on May 19, 2014.

APPROVED:

_____

Mentor, representing Mechanical Engineering

_____

Committee Member, representing Mechanical Engineering

_____

Committee Member, representing Mechanical Engineering

_____

Dean, University Honors College

I understand that my project will become part of the permanent collection of Oregon State University, University Honors College. My signature below authorizes release of my project to any reader upon request.

_____

Mitchell A. Daniels, Author

Acknowledgements

I would like to thank Dr. Vinod Narayanan for serving as my mentor throughout this project. His guidance served invaluable throughout the course of the thesis process. I would also like to thank Eric Truong for helping me with machining components and providing help throughout the entire process. Shashank Natesh also provided valuable help with editing and data processing. Without them this thesis would be nowhere near what it is today.

I must also thank my family Scott, Jan and Meaghan for their constant support during my education. In addition I would like to thank my friends Eric Walters, Andrew Miller, and Whitney Hopple for their help throughout my undergraduate career.

Table of Contents

List of Figures

List of Figures (Cont.)

List of Figures (Cont.)

List of Tables

Effects of Channel and Ratchet Geometry on
Passive Pumping in an Open-ended channel Configuration

1. Introduction:

Advances in technology have made electronics an integral part of modern society. With increased capability of electronic components, the heat produced also increases dramatically. This puts a greater demand on the cooling systems. Advanced cooling systems are needed to meet the new requirements for heat dissipation in advanced electronics. There are several cooling system designs commonly used in modern electronics including heat pipes, heat sinks, forced air convection, and heat exchangers with single phase liquid cooling.

A heat pipe consists of a working fluid that undergoes evaporation at the hot end. The generated vapor is transported in the hollow core of the heat pipe to the condenser. Liquid is then wicked back down to the heated end of the pipe through a mesh by capillary action. This is a common way of achieving two phase heat transfer in electronics. Two phase heat transfer is efficient due to the large amount of energy required to change the phase of a substance. Phase change is an isothermal processes so the temperature of the fluid can be maintained at a constant temperature in these cooling solutions.

A heat sink is a large piece of conductive material designed to conduct heat away from an electronic component. The heat sink is usually designed with fins to greatly increase the surface area. A fan is used to force air flow over the heat sink to facilitate convection heat transfer. This is the most common solution used in modern computers and is sometimes used in conjunction to heat pipes. Forced air convection is fairly efficient due to

convection having larger heat transfer coefficients than other heat transfer methods and the large surface area created by the heat sink. However, this method requires excess power to be inputted into the system to move the fluid, which results in a loss of efficiency. This solution also requires a larger area to operate efficiently and therefore is not used in modern smaller electronics such as smart phones.

Single phase liquid cooling is utilized in advanced electronics with large heat dissipation needs. Liquid cooling is more efficient than air cooling since liquids have a larger specific heat and thermal conductivity than air or other gases. It takes more energy to raise the temperature of a liquid a few degrees than a gas. This allows the liquid to remove more energy from the system. However liquid systems require more power input to pump the fluid through the pipes. Pumps generally tend to require more power input than fans. Liquids can also damage electronics, which requires excess components and design to prevent leakages. It also decreases the efficiency of the system because of the reliance of conductive heat transfer through a pipe or a channel. There are some fluids such as Fluorinert^{TM} FC-72 [1] in which electronics be completely immersed. However, special design is needed to prevent leakage outside of the system.

A large amount of modern electronics cooling research goes into improving liquid cooling systems. Modern electronics are starting to use liquid cooling systems. Companies have come out with liquid cool smart phone and CPU packages.

Work completed at Oregon State University by Kapsenberg [1] and later by Strid [2] has shown the feasibility of thermally actuated pumping for cooling electronics. This work showed that an asymmetric surface can cause the bubbles to depart at an angle. The bubbles then transfer momentum to the fluid causing a lateral motion of the fluid. Even

though it is currently still in validation, passive pumping of fluid has the potential to create a cooling solution with no excess power input needed and less complexity of a mechanical pump with the efficiency of two phase flow.

This thesis will build upon the work done by Strid [2] by testing the two phase pumping concept in a channel configuration.

2. Literature Review:

This section will review past work related to the motion of fluid boiling on ratcheted surfaces. The first part looks at research performed on the motion of droplets on surfaces due to the Leidenfrost effect. Then work on the motion of bubbles in pool boiling is discussed, followed by past work on the open-ended channel pump configuration.

2.1. *Leidenfrost Droplets:*

The Leidenfrost effect or film boiling is a phenomenon where a liquid in contact with a hot surface creates an insulating layer of vapor. This layer prevents the liquid from evaporating too quickly, as the main heat transfer mechanism becomes radiation [1]. The layer of vapor separates the liquid from the heated surface. In the case of a single droplet on a solid surface, the droplet can be suspended above the surface. This can be demonstrated easily by a few droplets in a pan. The droplets will move around the pan erratically.

Experiments were run on droplets of various liquids including nitrogen, acetone, methanol, ethanol, water, and hexadecane with boiling points ranging from -196 °C to 151 °C [1]. These droplets were placed on an asymmetrical ratcheted surface with different pitches varying from 0.1 mm to 0.3 mm maintained at a temperature above the Leidenfrost temperature of the liquid. Each liquid exhibited an induced motion perpendicular to the ratchet surface. A schematic of the Leidenfrost droplet on a ratchet is shown in Figure 1.

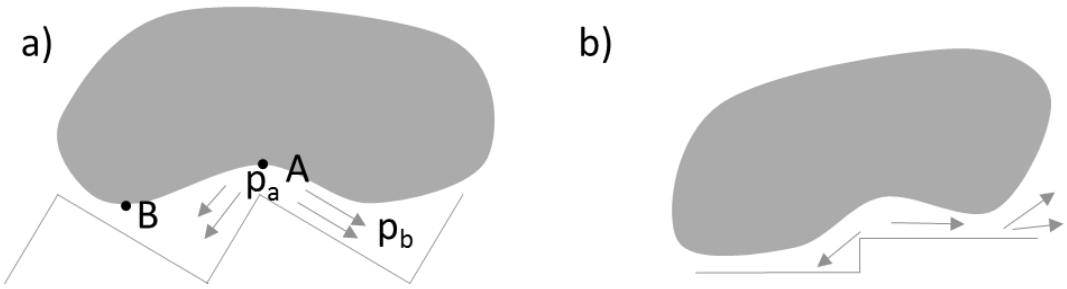

Figure 1: a) Leidenfrost droplet on ratcheted surface showing pressures and geometry. b) Droplets overcoming small obstacle.

Speeds up to 5 cm/s were observed for distances up to 1 meter. The distance was limited by the complete vaporization time of the droplet. The motion was enough to overcome the edge of a piece of tape with a height of 0.2 mm as shown in Figure 1b. Figure 1 also shows the vapor flow direction. Vapor flowing from A to B was observed to escape out the ratchet grooves, while vapor flowing forward met more resistance and dragged the liquid droplet along from left to right. This is why the two ratchet sides do not cancel each other out and a net motion is observed. It was also observed that bubbles with diameters smaller than the pitch of the ratchets would exhibited no motion and large diameter droplets tended to break up along the length of the surface.

The model proposed was that the motion is due to a viscous force exerted on the droplet. This is brought about by the shape of the bubble. Due to the ratchet, the bubble is concave at the ratchet peak and convex at every other surface. The differences in the curvature of the droplet can be used to estimate the change in dynamic pressure of the vapor. The difference between the internal pressure of the droplet (p_a) and the vapor (p_b) can be approximated by the equation:

$$\Delta p = \frac{\gamma}{R} \quad (1)$$

Where γ is the liquid surface tension and R is the radius of curvature for a local area of the droplet. Due to the differences in curvature, the pressure at the concave area of the droplet is higher than the convex areas. Vapor will want to flow from point A to B in Figure 1a due to this pressure gradient. The flow drags the droplet along due to viscous interactions. It was assumed that backward flow of the vapor was negligible.

The shear force driving the fluid can be modeled based on the equation:

$$F = .5A_{eff}h\left|\frac{dP}{dx}\right|cos\theta \quad (2)$$

Where A_{eff} is the total area that the force acts upon, h is the thickness of the vapor layer and θ is the angle of the ratchets. There is also a viscous drag force that opposes the motion of the droplet. This force is given by the equation:

$$F_d = -\left(\frac{\mu A_{eff}}{h}\right) * v_x \quad (3)$$

Where μ is the viscosity of the fluid and v_x is the velocity of the droplet.

The radius of the droplet and the thickness of the vapor layer were found using high speed video. The data collected was used to predict the acceleration of the droplet using the above model. It was found that the model agrees with the results within the experimental uncertainty.

Similar studies have been done on the motion of Leidenfrost droplets. Fenget al. [2] looked at the effects of different surface configurations on the motion of the droplets. They defined the Leidenfrost point (LFP) as the point when droplet transitioned to the film boiling regime. They found that the droplets travelled faster and lasted in the low temperature regimes. Thin film coatings were found to be effective in adjusting the LFP,

with hydrophobic surfaces increasing the LFP. Lagubeau et al [5] looked at measuring the force produced by these droplets. Forces on the drop were measured by a thin glass fiber that deflected when the drop caught it. The study found that the force by the drop imparted is a function of the radius of the drop. However the terminal velocity of the drop only slightly depends on the radius and is more a function of the ratchet geometry. It was also found that drops smaller than the ratchet pitch cannot move due to the Leidenfrost forces.

2.2. *Lateral Fluid Motion in Nucleate Boiling Through Asymmetric Surface Structures*

The purpose of these experiments performed by Kapsenberg [1] and Thiagrajan was to test the feasibility of initiating preferential liquid motion through passive asymmetric structures [4] [5]. The experimental set up consisted of a surface of silicone ratchet structures with reentrant cavities with a face angle of 24° from the horizontal. The structures were constructed using gray scale lithography and deep reactive ion etching. A thin film aluminum heater was placed below the structure to supply a heat flux. Figure 2 shows a diagram of the test section set up with applied heat flux. Data collection was achieved using high speed video and a custom bubble tracking algorithm.

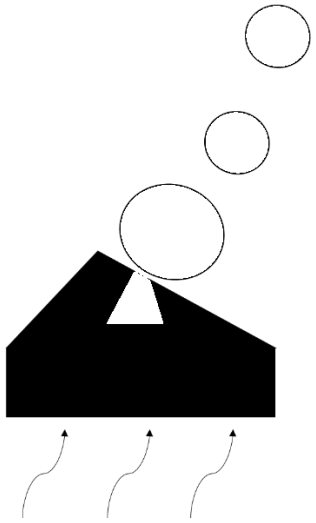

Figure 2: Diagram showing geometry of ratchets and re-entrant cavities and bubble motion.

The low subcooled test used deionized, degassed water at atmospheric pressure with 5 °C subcooling and an applied heat flux of 1.96 w/cm^2. Qualitatively, this test saw large well focused bubbles that tended to grow due to low temperature gradients. The bubbles grew at the cavities and departed at an angle normal to the face but then quickly rose upwards due to larger buoyant forces, therefore not much velocity was imparted to the pool. Velocity analysis showed unsteady velocities near the ratchet surface are present due to oscillations caused by coalescing or detaching bubbles.

The second set of tests used water with 20°C of subcooling at an applied heat flux of 18.94 W/cm^2. The images collected were much more distorted due to density differences caused by temperature gradients. Bubbles were observed to depart at high speeds with only a small upward component of velocity. Velocity analysis showed the bubble initially departs at speeds in the range of 170 to 200 mm/s. When the bubbles departed, they collapse rapidly due to the large subcooling in the pool and can accelerate rapidly to speeds up to 906 mm/s. This high speed allowed for the departure frequency of the

bubbles (f_d) to be measured as 320 Hz. The bubbles then slow downed to 200 mm/s once fully collapsed and then slowed to 30-60 mm/s once entered the plume of the pool with a horizontal component of 25-35 mm/s. Figure 3 shows the tracking algorithm used to retrieve the velocity data and visually presents some of the results of the tests.

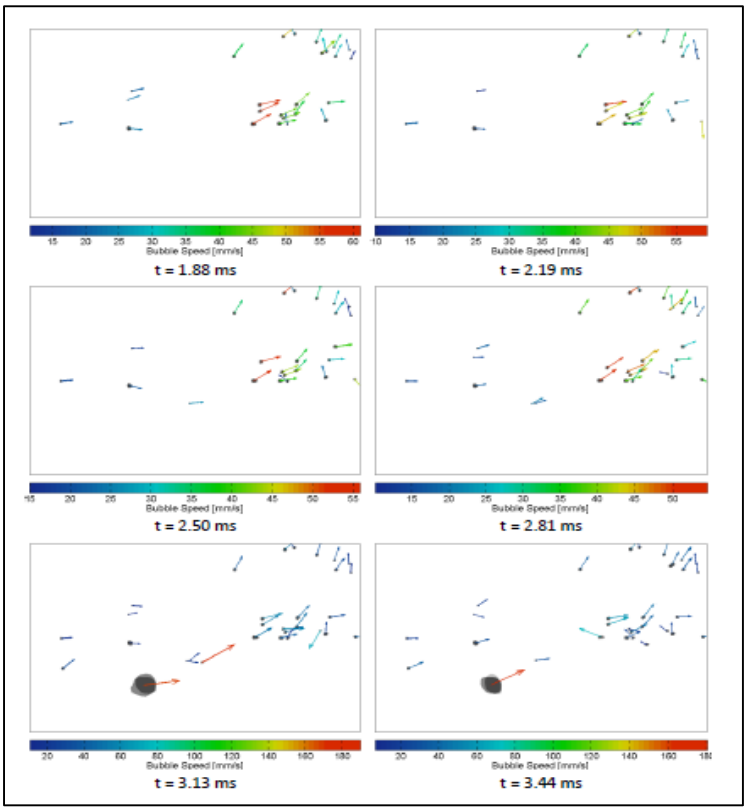

Figure 3: Series of video stills showing the results of the bubble tracking algorithm. Adapted from [4]

Kapsenberg, et al [7] developed a proposed model for the velocity of bubble. The model was derived from the conservation of momentum between the bubble growth and a control volume of liquid above the cavities. It was assumed that the bubble remains a sphere and the control volume cross section area is $1/28^{th}$ the area of the total test section or A_{ts}. The drag force displaced by the bubble was used to calculate momentum based on

its time rate of change and then the momentum was equated to the mass of the control volume liquid multiplied by the velocity.

$$-F_g = \frac{dP_i}{dt} = \frac{1}{8}\pi\rho_l C_d d^2 \left(\frac{\partial \vec{h}}{\partial t}\right)^2 \tag{4}$$

$$\bar{P}_l = \frac{1}{8}\pi\rho_l \sum_{i=t0+1}^{tf} C_d \left(\frac{d_i + d_{i-1}}{2}\right)^2 \left(\frac{h_i - h_{i-1}}{dt}\right)^2 dt \tag{5}$$

$$\bar{P}_l = m_l \bar{v}_l = \left(\rho_l A_{inf} f_d^{-1}\right)(\bar{v}_l) \tag{6}$$

Solving the equations yielding the model for the velocity of the fluid.

$$\bar{v}_l = \sqrt{\frac{\pi f_d}{8A_{inf}} \sum_{i=t0}^{tf-1} C_d a \left(\frac{d_i + d_{i+1}}{2}\right)^2 \left(\frac{h_i + h_{i-1i}}{dt}\right)^2 dt} \tag{7}$$

The model predicts a velocity of 45 mm/s with a horizontal component of 18 mm/s. This was reasonably close (within 33%) to the measured values of bubble velocity during validation tests. This suggests that the model may predict the driving force of the motion accurately.

2.3. *Open-Ended Channel Pump:*

All of the previous work done involving the motion of bubbles departing from an asymmetrical passive surface has focused on one surface immersed in a pool. A new

application of the principles explored previously is an open-ended channel pump configuration [6]. The channel consists of two ratchets on either side placed so that the preferential direction of the fluid are in the same directions. The channel width can be adjusted to create different hydraulic diameters. The channel had a height 3.175 mm and widths tested were 4.5 mm and 2.25 mm.

Several different flow behaviors were observed in the channel during the tests. The first is described as churn flow. Churn flow consists of large erratic bubbles that travel quickly through the channel Figure 4. The bubbles observed were unstable, have irregular edges, and tend to merge and depart randomly. This is shown in figure 6, as the bubble travels to the right several smaller bubbles from and combine into a large slug. Churn flow was observed for tests with high heat flux and moderate subcooling (15-30 °C) with a 4.5 mm channel. Velocity of the slugs was observed to jump to high values during bubble mergers and generally was observed to be chaotic and sometimes reversed directions.

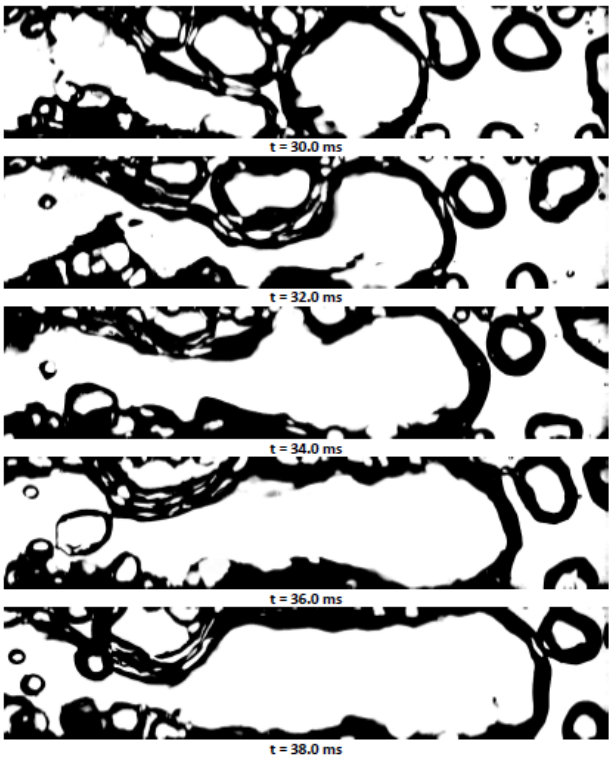

Figure 4: Video still data from experiment showing churn flow regime [6].

The second flow pattern observed is labeled as intermittent slug flow. This flow regime is cyclic in nature. Bubbles begin to grow then coalesce and accelerate down the channel when they reached the opposite ratchet surface, figure 4. Velocities observed were fairly consistent, except for intermittent large spikes due to vapor slugs merging. This pattern was observed for a large array of conditions, which are listed below

- P=1.009±0.058 bar, ΔTsub = 17.7 ± 1.73 °C, 1.37 ± 0.04 W1cm-2, w=4.5 mm
- P = 0.998 ±0.058 bar, ΔTsub = 26.8 ± 1.73 °C, 1.37 ± 0.04 W1cm-2, w=2.25 mm
- P = 0.572 ±0.058 bar, ΔTsub = 5.8 ± 0.4.5 °C, 0.58 ± 0.02 W1cm-2, w=4.5 mm

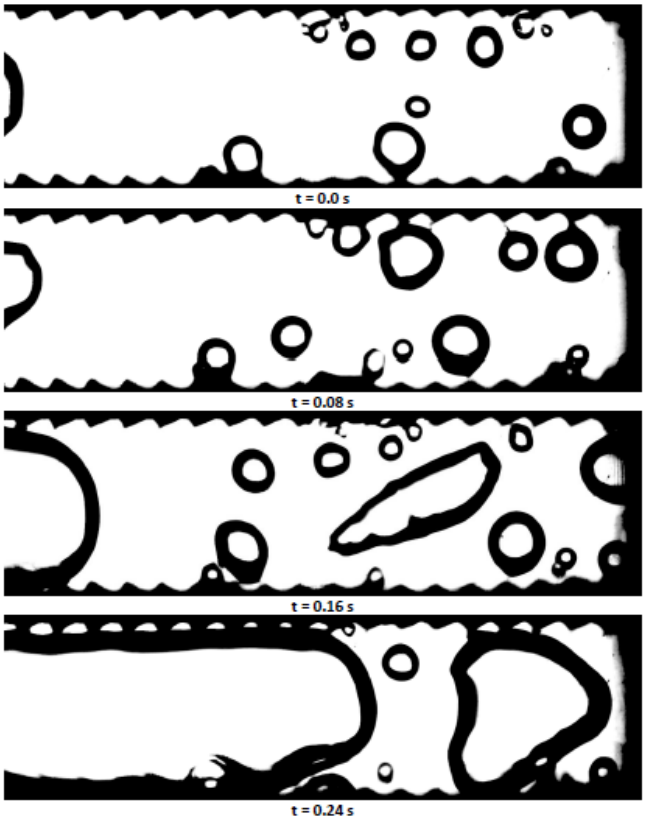

Figure 5: Video still data from experiment showing intermittent slug flow regime [6].

The third type of channel flow observed was labeled as walking bubble flow. This flows consists of large bubbles that appear to roll or bounce along the surface of the channel. The bubbles collect smaller bubbles and grow along the channel length but were never observed to expand to the size of the vapor slugs observed in other flow channels. This flow occurs in conditions where rapid bubble production is difficult. The velocities observed are less unstable than the intermittent slug and churn flows due mainly to fewer major bubble mergers and no flow reversal. Video stills of the walking bubble flow regime are below presented in Figure 6.

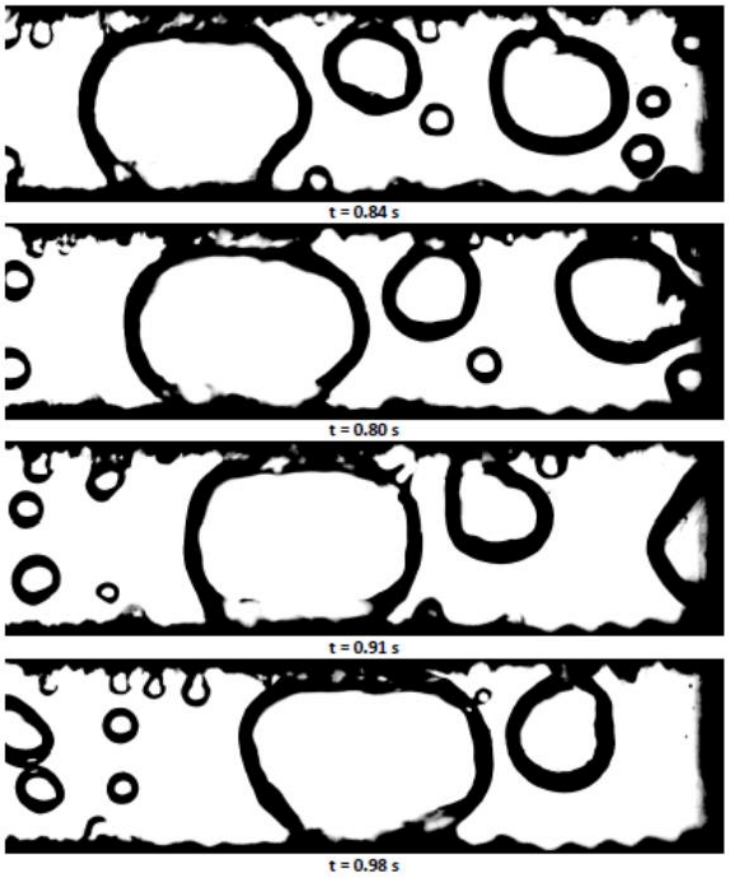

Figure 6: Video still data form experiment showing walking bubble flow regime [6].

The final flow regime observed was homogeneous slug flow. This flow occurred under flash boiling conditions (subcooling of -0.5 °C) caused by low chamber pressures. Slug departure was observed to occur at consistent intervals. The slugs grew in both directions and then accelerated rapidly down the channel when it reached a size of about one-third to one-half of the channel width. Velocity data showed that the slug velocity behaves in a linear manner. This shows that the slugs accelerate at a constant rate. Figure 7 shows a series of video stills from a test that represented the homogenous slug flow regime.

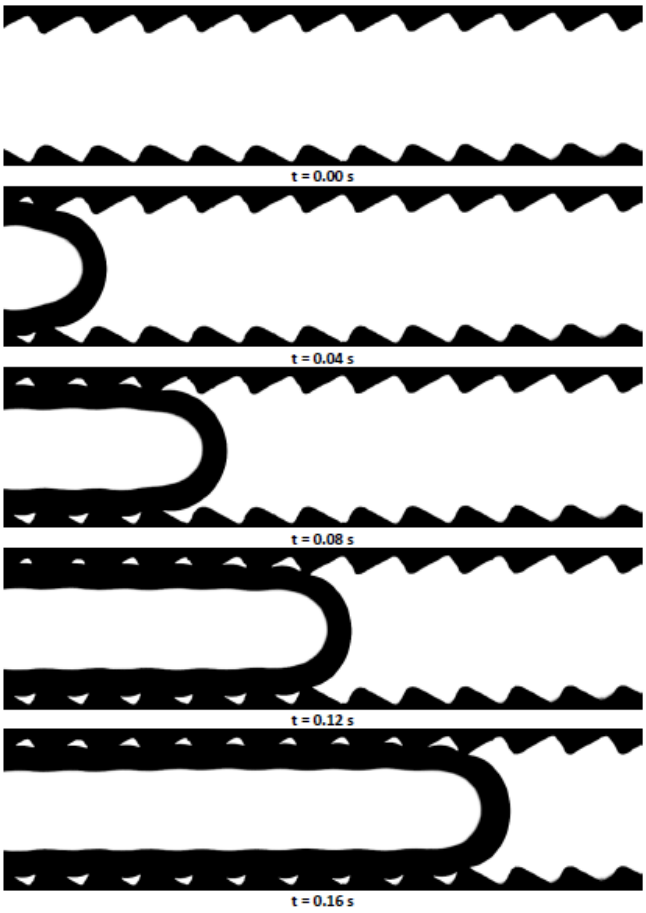

Figure 7: Video still from experiment show homogeneous slug flow regime [6].

The suggested model for the motion of the slugs through the channel is based upon a pressure differential in the fluid layer. A thin layer of fluid was observed between the interface of the bubble surface as shown in Figure 8.

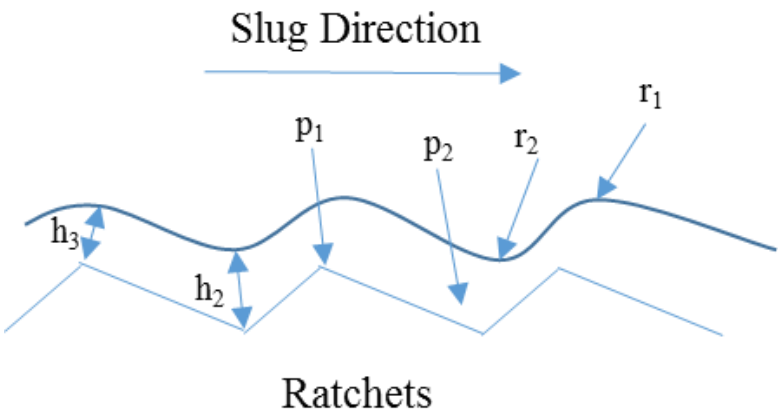

Figure 8: Illustration of proposed pressure model to explain channel flow.

The shape of the ratchets create differing pressures along the direction of the slugs. This differential can be found using the Young-Laplace equation.

$$P_{1,l} - P_{1,v} = \frac{\sigma}{|r_1|} \tag{8}$$

$$P_{2,l} - P_{2,v} = \frac{\sigma}{|r_2|} \tag{9}$$

Where P_v denotes vapor pressure, P_l denotes liquid pressure, σ denotes the surface tension. And the subscripts 1 and 2 are as shown in Figure 8. Solving for the differences in the liquid pressures yields:

$$P_{2,l} - P_{2,l} = \sigma\left(\frac{1}{r_1} - \frac{1}{r_2}\right) \tag{10}$$

2.4.*Conclusions from literature review*

There have been several studies done on the effect of asymmetric ratcheted surfaces on droplet. These studies showed a preferential direction of the droplets along the surface depending on the shape of the ratchets. Kapsenberg [4] and Strid [6] looked at pool boiling applications of these surfaces. These studies showed preferential direction of bubble and fluid flow in the pool. Kapsenberg proposed a semi-empirical model for the bubble motion, which was later refined by Strid. Strid also applied the principle to an open-ended channel pump configuration [6]. This test showed similar preferential direction of the bubbles along the channel with different bubble behavior depending on the heat flux and sub cooling conditions. Strid's work only considered two forms of channel geometry, with varying heat flux. Only one parameter of the channel configuration was tested. It was also observed that the channel geometry did not allow for the bubbles to fill the entire channel. Bubbles would float and only fill the top part of the channel. Further work is needed to study the influence of channel and ratchet geometry to further validate the concept of an open-ended channel pump.

3. Scope and Objectives:

This thesis will expand the work on the boiling with ratcheted surfaces in an open-ended channel pump configuration. The study will look at how the channel and surface geometry affects the motion and behavior of the bubbles. The goal of this study is to test which geometrical parameters affect the performance of the open-ended channel pump concept. The channel height will also be reduced from previous studies. This will allow the bubbles to fill the entire channel, instead up floating to the top. Table 1 shows the geometry to be tested during this study and offers a brief description of each geometry.

Table 1: Geometries and channel widths to be tested during this study.

Geometry	Asymmetric	Asymmetric	Symmetric	Partially Flat	Fully Flat	Offset
Width	1.5 mm	1.0 mm	1.5 mm	1.5 mm	1.5 mm	1.5 mm
Description	One shallow face, one steep face. Similar to past experiments	One shallow face, one steep face. Similar to past experiments	Equal Angles, Baseline to compare asymmetric	Asymmetric ratchets with intermittent flat regions to test interactions	Baseline to compare effect of ratcheted surface	Crests offset by half a pitch.

In order to carry out this study a test chamber was constructed to house the channel configuration test section. This chamber has the ability to adjust the width of the channel and the house different ratchet geometries a local heat flux will be applied to the surface of the ratchet in a reduced pressure environment. Pressure of the chamber and the temperature of the pool will be monitored and recorded. High speed video will be used to observe the bubble formation and motion.

4. Experimental Facility:

This section discusses the equipment used during testing. The first subsection discusses the test section and ratchets. The second discusses the chamber used to house the experiment. The final subsection discusses the peripheral equipment used to take data and support the experiment.

4.1. *Test Section*

This section describes the section used for the experiments. The test section consists of a rectangular open-ended channel with an adjustable width. Each wall of the channel consists of ratcheted structures. The chamber ceiling and floor are clear to allow for imaging and light to pass through for data collection. The ratcheted surface is attached to an insulator with a heater sandwiched in between. Figure 9 shows the test section as tested with the insulator, heater, and ratchet.

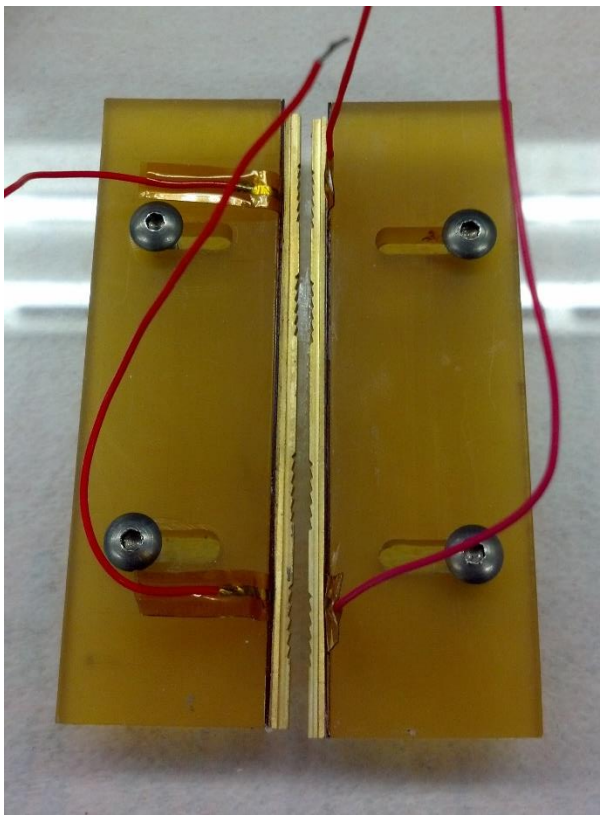

Figure 9: The test section set up showing the insulator, the heater leads, and the ratchets.

The ratcheted surface is machined from brass and then sand blasted. The detailed geometry used in this thesis is shown in Figure 10.

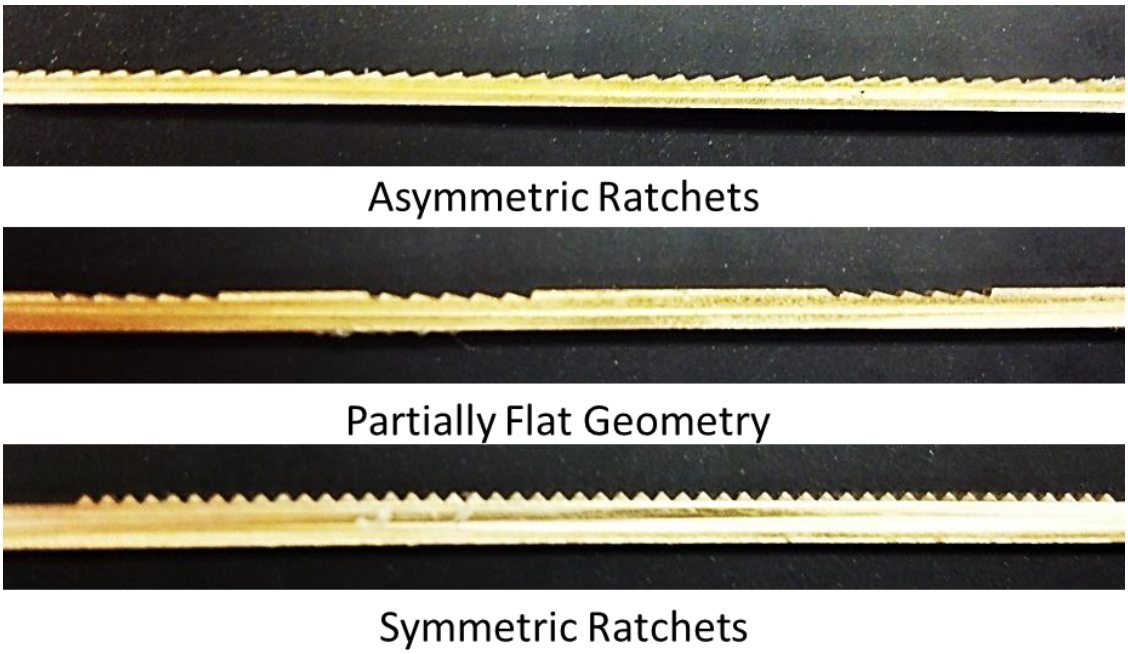

Figure 10: Detailed view of ratchet test section showing the different geometries used during testing. Asymmetric ratchets consist of 30°-60° sides. The partially flat geometry has the similar asymmetric ratchets spaced by flat regions. The symmetric ratchets are 45° on each side.

The structures used consist of several different ratchet shapes. Each ratchet section was approximately 1.5 mm in height and 76.2 mm long with a pitch of around 1 mm. The structures were aligned in the channel as mirrored images so as to create a preferential direction for the bubble growth and departure; except in the offset tests the ratchets are offset by half a ratchet pitch, but still mirrored to create the preferential direction. The ratchets are mounted to the insulator and heater using double sided Kapton® tape.

The insulator is made from polyetherimide (Ultem 1000 [8]) and measures 76.2 mm by 25.4 mm by 5.5 mm. It is bolted to the bottom of the test chamber using #4 machine screws. Slots machined into insulator allow the width of the channel to be adjusted by simply sliding the pieces to the desired width apart. The material has a low thermal conductivity to ensure most of the heat from the thin film heater is transferred to the

ratcheted surface. Polyetherimide also has a high heat deflection temperature which prevents the part from becoming damaged after continued usage.

The heater is a piece of Iconel Alloy 600 foil cut into a serpentine with a thickness of 0.001 inches. Large leads are cut into the foil to prevent heat being generated at the leads. The heater is then placed between two layers of Kapton tape in order to give strength and prevent tearing. The tape also provides a dielectric barrier from the working fluid in the chamber. The heater assembly is attached to the insulator using double sided Kapton tape and then sandwiched by another piece of tape to attach the ratchet test section. A polycarbonate piece with a rectangular cross section is used to seal the top of the test section from the rest of the chamber. This is achieved by compressing the piece with the top of the chamber. The piece was 76.2 mm long with the height and width dependent on the ratchet height and the channel width required for the test.

4.2. *Test Chamber*

This section describes and discusses the chamber used to house the experimental test chamber. Figure 13 shows the fully assembled chamber used for testing.

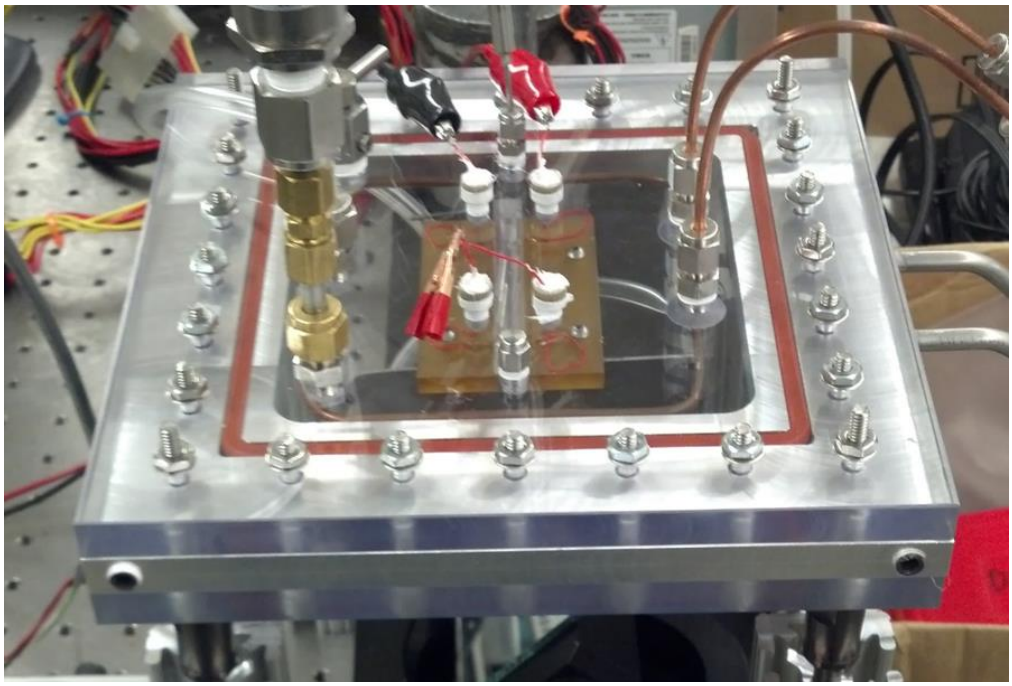

Figure 11: Fully assembled test chamber showing the ports for various peripheral equipment, the O-rings used for sealing, and the test section.

The top and bottom pieces are made from transparent polycarbonate measuring 216 mm by 216 mm by 12.7 mm. Transparency allows for light to pass into the chamber and images to be taken from the bottom of the chamber. The middle section is aluminum with outer dimensions of 216 mm by 216 mm with a 127 mm by 127 mm section machined out in the middle and is 12.7 mm thick. This section has O-ring grooves machined into the top and bottom surfaces. The O-rings are designed to seal the chamber when a vacuum is pulled on the inside. Silicone O-rings with a cross section diameter 5.2 mm and an inner diameter of 279.4 mm. Bolts and nuts are used to attach the three pieces and ensure sealing of the O-rings. Nuts are used to clamp down instead of threaded holes because polycarbonate is soft and the threads can easily be stripped by the force of the O-ring.

The top piece of the chamber has ports drilled and tapped to interface with peripheral equipment. The wires are fed through fittings that are then sealed up using silicone rtv sealant. A needle valve is used to fill the chamber with the working fluid, FC-72. Copper $1/8^{th}$ inch pipes run through two compression fittings at the top and are used as condenser coils to maintain pressure in the experiment. Other ports include ports for thermocouples, a vacuum pump, and a pressure transducer.

4.3. *Test Facility*

This section discusses the peripheral equipment used to support the test and measure data. The stand for the test chamber consisted of four 80-20 extruded aluminum posts with sheet metal brackets to hold them together. Fine threaded (1/4”-80) caps are threaded to the top of the posts with ball bearings on top of the caps. Bolt heads at each corner of the chamber rest on the ball bearings; this allows for fine adjustment of the height of each corner. Underneath the stand is an adjustable mirror which allows for imaging of the bottom of the test section. The mirror measures 85 mm by 65 mm and is supported by a stands that allows for adjustments of the angle. Figure 12 shows the stand set up without the chamber.

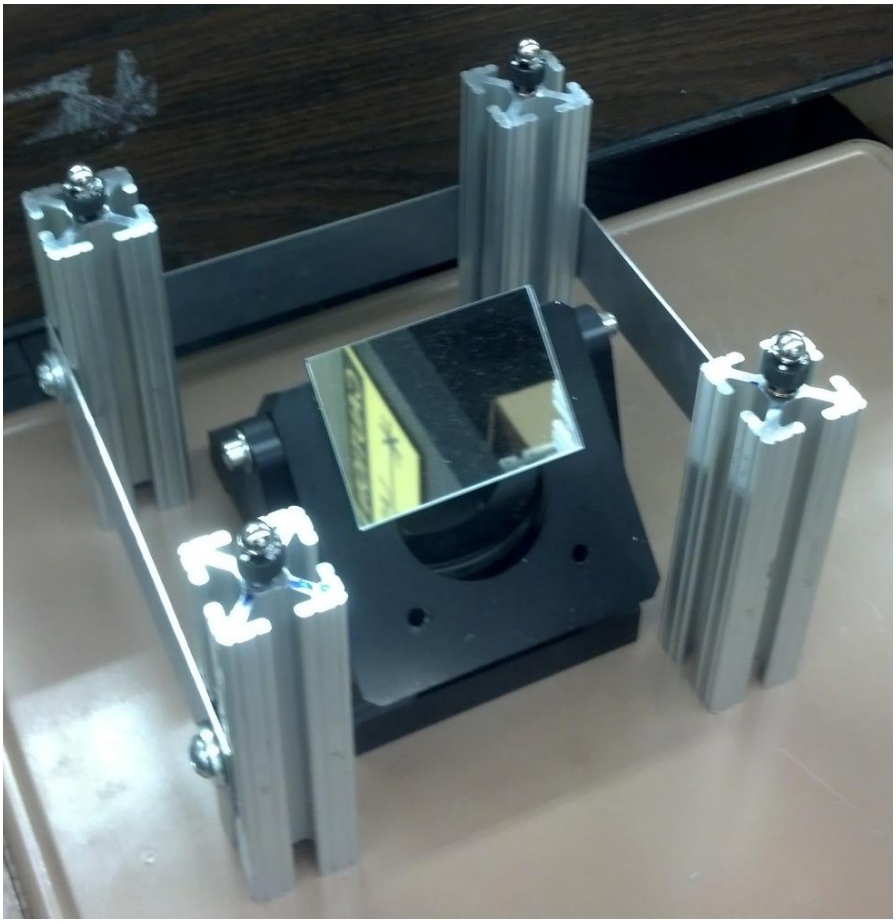

Figure 12: Stand used to support the chamber. The chamber sits on the ball bearings which allows for fine adjustment of the height. The mirror underneath is used for imaging of the bottom.

An Omega PX302-100AV and Omega K-type thermocouples are used to monitor the conditions inside the chamber using a Labview VI. The pressure and temperature data is used to get the subcooling condition of the pool during a test. A vacuum source is attached to a Welch Scientific Duo-Seal Vacuum Pump in order to adjust the pressure inside the chamber. The condenser coils in the chamber are hooked up to a Thermo Haake C30P chiller. The chiller pumps fluid at -20 °C through the pipes to help condense the vapor produced during the experiment. A Circuit Specialists CSI 33035 DC power source is used to supply a heat flux to the heaters. A large LED array is used to illuminate

the chamber for imaging. The array consists of 625 white LEDs in a 25x25 grid measuring 127 mm by 127 mm.

High speed imaging is achieved using a Phantom v310 camera. This camera was selected due to its ability to record at a high rate (up to 500,000 fps) and a high resolution (up to 1280x800). The camera is mounted on a T-slotted aluminum rail with a length of 92 cm in order to be able to adjust the position. Vision Research's Phantom Camera Control (PCC 1.3) software is used to monitor the video and save images. Figure 15 shows the camera used and the rail mount.

Figure 13: v310 high speed camera mounted on slide rail to allow adjustment of the position.

5. Experimental Procedures

This section lists the procedures used for conducting tests using the experimental set up. The first subsection discusses the procedure for set up. Then the procedure during testing is discussed, followed the procedure for shutting down the facility.

5.1. *Set-Up Procedure*

Once the ratchet test sections were machined, they were taped off and then the front surface was sandblasted. The ratchets were then cleaned with isopropyl alcohol to remove any residue from the previous tests and the sandblasting process. Then the ratchets were placed in a sonic cleaner for fifteen minutes. Once out of the sonic cleaner, the test sections were wiped down with isopropyl again to ensure no residue is left on the ratchet.

When the ratchets are fully cleaned, double sided Kapton tape was used to attach the ratchet to the insulator. The two sides of the test section are pressed together in order to ensure proper bonding. A small amount of silicone RTV is used to seal the bottom of the test section. This was achieved by placing a small trail of the RTV and then smoothing it out to ensure a flat bottom and good sealing. Dowel pins that are a precise diameter were used to line up the channel width. The pins were placed between the two sections, which were then pressed together and bolted into place. The appropriate ceiling piece is then placed on top of the test section.

Once the test section is fully assembled and mounted on the bottom plate of the chamber, the middle and top plate of the chamber were then placed into position. The wire leads for the heaters were fed through the fittings in the top of the chamber. The four corners bolts were finger tightened onto the chamber in order to ensure proper alignment of the assembly. Silicon RTV was then used to seal the wire ports. The chamber was then left to set for at least 3 hours in order to ensure the RTV was dried and sealing occurred. Next, the chamber was bolted together. The bolts in the middle of each section were tightened first to ensure even sealing of the ceiling piece, followed by the bolts in the four corners. Then, the rest of the bolts were tightened up to ensure good compression of the O-rings.

The chamber was then placed onto the stand. The chiller was then attached to the condenser pipe fittings and tightened to ensure no leaks. The chiller is then turned on to begin the cooling and pumping cycle. This ensures ample time for the chiller fluid to be cooled to the set value of -25°C during the set up process. Next the pressure transducer and the vacuum pumped are connected to the chamber using compression fittings and were tightened to provide good sealing. The thermocouple was then connected and the power supply to the transducer was then turned on. The Labview VI program was started to ensure the transducer and thermocouple are reading correctly. Writing of data to a text file was then initiated.

The software for the camera was then opened. Power was connected to the camera and after about a minute the Ethernet cable was also connected to the camera. The camera was selected in the software and a current session reference was performed with the cap on. The LED array was switched on and then the camera cap was taken off. Then, the mirror and stand position was adjusted until the image of the test section was centered

and level within the 1280x152 resolution image frame. The sampling rate was changed to 1000 frames per second.

A Spi Tronic PRO 360 digital level with an accuracy of 0.1° was used to check the orientation of the chamber. The level was held to the bottom of the chamber. The height of the post was adjusted until the level read 0.1° one way, the position of the adjuster was noted. The height was then adjusted further until the level read 0.1° the other way with the position again noted. The knob was then adjusted to a position between the two points noted earlier. This ensured that the tilt of the chamber was as close to 0° as could be obtained with the level. The process was repeated for all the sides of the chamber.

A valve to the vacuum source was then opened up slowly to drop the pressure inside the chamber to about 0.3 bar and then closed. The pressure was monitored for about a minute to check for any vacuum leaks in the system. FC-72 was then pulled into the chamber from a 120 ml glass container due to sub atmospheric pressure inside the chamber. FC-72 was added to the chamber until the fluid level was just above the top of the ratchets, or approximately 35ml. Once the chamber was filled, the orientation was checked one more time with the digital level before testing began. Testing began once the temperature and pressure of the chamber remained within 0.1°C or 0.01 bar respectively for two minutes.

5.2. *Experimental Procedure*

To begin testing, the valve to the vacuum source was opened to lower the pressure until the pressure was below the saturation pressure of FC-72 and boiling began. Video of the flash boiling was recorded and saved. The valve was then closed off. Power was supplied

to the heater and the voltage and current was adjusted to a 4W input, then 3W, then 2W and then 1W. Once these steps were completed the power was decreased to a low amount, usually around 0.5W depending on the amount of bubble activity observed at lower power. Then the power was increased again to higher power inputs. This was done in order to see if similar conditions could produce similar behavior in both directions. Video was captured for each power input. Then, 5000 frames of the video was selected to be saved in ordered to observe a wide range of data while still minimizing file size. The process was repeated for each geometry orientation. Table 2 shows the test matrix of all the power input points collected for each geometry orientation.

Table 2: Test matrix showing the power inputs at which video was captured for each geometric orientation

Ratchet	Symmetrical	Asymmetrical			Flat	Partially Flat	
Offset	Yes	No	Yes	No	No	Yes	No
Width	1.5 mm	1.5 mm	1.5 mm	1 mm	1.5 mm	1.5 mm	1.5 mm
Heat Input	Flash Boil	Flash Boil	Flash Boil	Flash Boil	Flash Boil	Flash Boil	Flash Boil
	4 W	4 W	4 W	4 W	4 W	4 W	4 W
	3 W	3 W	3 W	3 W	3 W	3 W	3 W
	2 W	2 W	2 W	2 W	2 W	2 W	2.5 W
	1.5 W	1.786 W	1.786 W	1.5 W	1.75 W	1.5 W	2 W
	1 W	1.5 W	1.5 W	1.25 W	1.5 W	1 W	1.5 W
	0.5 W	1.25 W	1 W	1 W	1 W	0.8 W	1 W
	0.1 W	1 W	0.5 W	0.25 W	0.5 W	0.5 W	0.8 W
		0.5 W	0.25 W			0.25 W	0.25 W
			0.1 W			0.1 W	0.1 W

5.3. *Shut down Procedure*

Once the run was completed the power to the heater was turned off and disconnected. The Labview VI and the camera software were then shut down. The Ethernet cable was unplugged from the camera and then the power cable after about a minute to allow the camera to cool off. The chiller was then shut off and disconnected from the chamber. To vent the vacuum, the needle valve was opened and then closed once the chamber has depressurized. Then, the pressure transducer and the vacuum source were disconnected. The FC-72 was drained by opening the valve, lifting the chamber and then draining the fluid back into the glass container. Then, the chamber was ready to be disassembled. Each bolt was loosened by half a turn in order to prevent warping of the sealing piece, and then taken fully off. The dried RTV was then removed from the wire ports. The top and middle plates of the chamber was removed. The test section was dismounted from the bottom plate of the bottom plate of the chamber. The ratchets are then taken off the insulator by using a razor to peel the test section off the tape. The tape and heater leads were then replaced as needed.

6. Data Analysis

This section discusses the processes used to create and analyze data collected. The first section discusses the selection process used to choose comparison points for the tests. The second section discusses the methods used to process the video data and retrieve bubble position data. Then the process used to analyze the number of events during high heat flux tests. The final section discusses possible sources of uncertainty and presents the analysis of the uncertainty.

6.1. *Selection Criteria for Further Analysis*

A large amount of data was collected while running the test matrix presented in Table 2. This data consisted of 36 videos consisting of 5000 images. Processing this amount of data can be cumbersome and impractical. In order to measure the effects of the channel geometry, it is important to compare data points with similar input conditions. To visualize the collected data the heat flux inputted was plotted against the subcooling of the fluid pool. The subcooling is measure temperature of the pool subtracted from the saturation temperature of the fluid at the measured pressure. Figure 14 shows the plot used for selecting data points for further analysis.

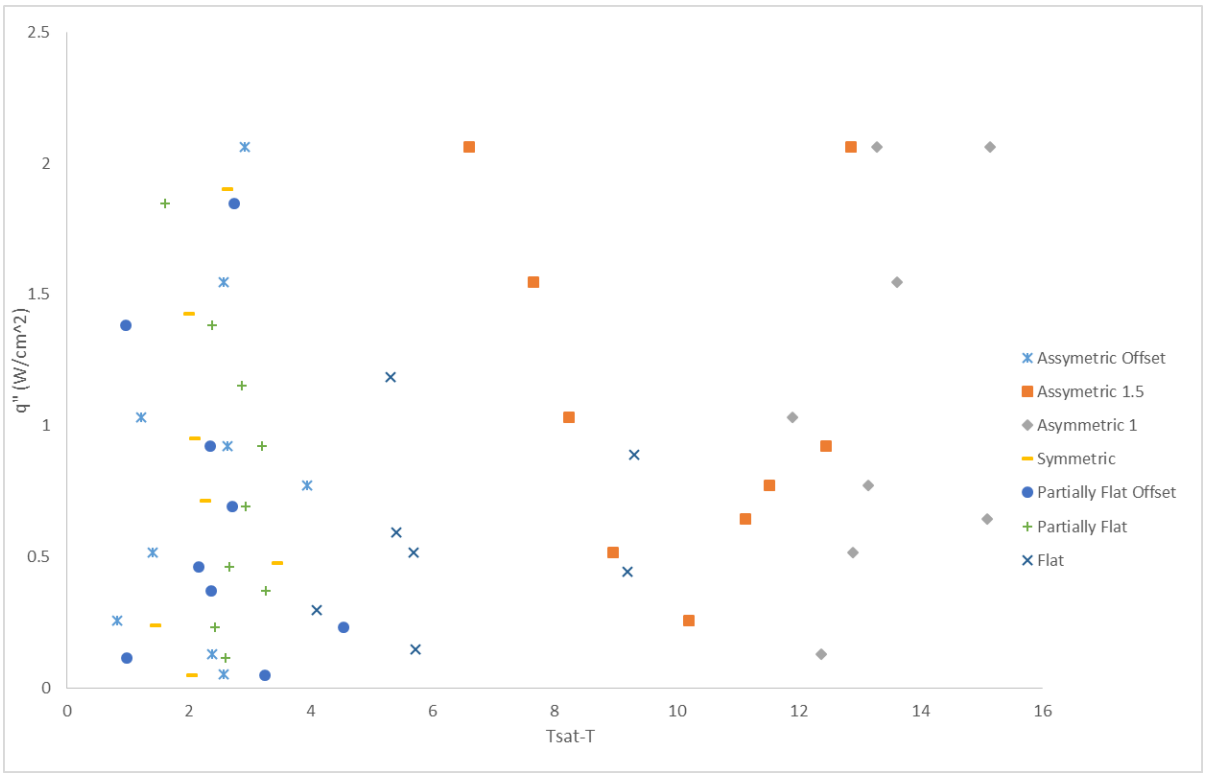

Figure 14: Heat flux inputted into the ratchet test section plotted against the subcooling condition (Saturation Temperature-Measured Temperature) for each of the different geometric configurations tested.

In order to compare different configurations points that are close together in Figure 14 are chosen for further analysis. Two points were chosen for analysis to compare each geometric consideration, one high heat flux input and one low. This analysis includes video processing in order to gather position data of bubbles as well as recording the number of venting events in order to quantify the boiling activity. Table 3 shows the conditions of the trials selected for further analysis.

Table 3: Conditions of trial runs used to compare the effect the geometric conditions on the behavior of the bubbles. Runs with similar conditions were chosen to achieve accurate comparison

Channel Width					
Geometric Condition	q" (W/cm^2)	T-Tsat (°C)	Geometric Condition	q" (W/cm^2)	T-Tsat (°C)
1.5 mm Channel Width	0.99	12.45	1 mm Channel Width	1.11	11.9
1.5 mm Channel Width	2.22	12.87	1 mm Channel Width	2.22	13.29
Offset Ratchets					
Offset Ratchets	0.76	2.71	Normal Ratchets	0.76	2.93
Offset Ratchets	2.02	2.75	Normal Ratchets	2.02	1.62
Flat Geometry					
Asymmetric Ratchets	0.28	0.82	Partially Flat	0.13	0.9784
Asymmetric Ratchets	0.99	2.64	Partially Flat	1.01	2.35
Partially Flat	0.25	4.54	Flat	0.30	4.1
Asymmetric Ratchets	0.56	8.96	Flat	0.44	9.2
Symmetric Ratchets					
Asymmetric Ratchets	0.99	2.64	Symmetric Ratchets	0.91	2.27
Asymmetric Ratchets	0.14	2.38	Symmetric Ratchets	0.06	2.06

6.2. *Slug Tracking*

In order to obtain information on the growth and travel of slugs image analysis software is used. National Instruments Vision Assistant software was used to process the video frames collected during the tests. This software is used to isolate the slugs and obtain information on the center of mass, the left bound, and the right bound.

The first step of processing the image was to import an avi format file and apply an image mask to the frames. The image mask blocks out the extraneous parts of the image and isolates the channel of the test section. A color threshold is then applied to the image. This step converts the 64-bit RGB format into an 8-bit binarized image which helps isolate objects. The binary image is then inverted, this makes the inner surface of the

bubble an object that can be tracked using the software. The inner edge is used because the outer edge of the slug is indistinguishable from the ratchet surface. Another method considered was using the fill holes filter in order to isolate the slug; however this method did not produce clear isolation due to the interaction between the channel walls and the slug. Once the image was inverted particle filters were applied to remove small objects. Figure 15 shows the original image and the steps used to process the image for analysis.

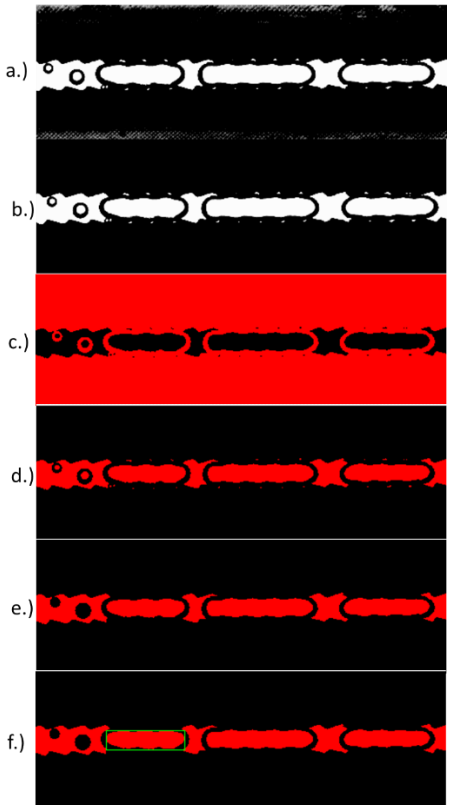

Figure 15: a.) Original image taken from a frame of an avi file. b.) Applying image mask. c.) Apply color threshold to binarize the image. d.) Reversing the image to track inside edges and separate slugs. e.) Removing small objects to remove some objects not of interest. f.) Particle tracking of a slug with bounding rectangle.

The downside of the image inversion method was that it does not fully isolate the slugs. There are generally several objects left on the image that are not of interest. This means that the image cannot be batch processed as this would produce large amounts of

extraneous data and the data of interest would be difficult to filter out. The output of the program for the position data is in pixels. In order to convert this data, the length of the ratchet is measured in pixels and then used to convert into mm from the known length.

6.3. *Bubble Venting Event Analysis*

Under certain conditions, like high heat inputs, a large slug that takes up the entire channel is formed that vents out the channel. The slug is fed by vapor formed from the heated surfaces. This makes it impossible to measure the growth and speed of the slug to quantify the behavior. In order to measure the behavior the number of times the slug vents into the pool will be measured. Both sides will be looked at in order to quantify preferential direction. If one side has many more events than the other, then this suggests a preferential direction to the chamber. The number of events can also indicate the amount of activity in the channel.

To run this analysis a Matlab script is written to measure the pixels values of a line profile at each end of the channel. It was observed that when the bubble vents the pixel values change. One method considered was to look at the dark bands at the edges of the image, because it was observed that these bands become white during an event. However, it was also observed that these bands also fluctuate when the slug pushes towards the edge of the channel but does not actually vent. The method for the script that was selected looks at the white area just outside the edge of the channel. When an event occurs the bubble edge shows up as black pixels that can be measure by the script. The script measures when the value of a pixel in the line first changes to zero and adds to a

count of the events. Figure 16 and Figure 17 show an example of the line profile used to measure the occurrence of an event.

Figure 16: Line profile used to measure when a slug venting event occurred on the right side of the channel

Figure 17: Line profile used to measure when a slug venting event occurred on right side of the channel during a venting event

6.4. *Uncertainty Analysis*

There are uncertainties associated with the measured values for slug position, time increment, pressure, temperature, and input heating. These uncertainties were propagated through calculations using the Kline-McClintock method.

An Omega PX302-100AV pressure transducer was used to monitor the pressure of the chamber. This pressure transducer has a manufacture specified accuracy of 0.25% full scale range or 0.017 bar [7]. The k-type thermocouple set up was calibrated in [6], and the uncertainty was determined to be 0.14°C. The uncertainty in the saturations temperature is assumed to be around 0.01°C. This was found by running a quick sensitivity analysis by varying the pressure in the program used to calculate the saturation temperature.

The uncertainty in the heat flux is dependent on the uncertainty of the caliper and the power source. The caliper uncertainty is assumed to be the resolution, about 0.01 mm. The uncertainty in the power is assumed to be the manufacturer supplied bias for the power supply, ±0.11 V for the voltage and ±0.011 A for the current. The total uncertainty is given by the equation:

$$u_q = \left(\left(\frac{V}{A} u_I \right)^2 + \left(\frac{I}{A} u_V \right)^2 + \left(-\frac{IV}{A^2} u_A \right)^2 \right)^{\frac{1}{2}} \tag{11}$$

Since the subcooling and the heat flux input were used to select points; this uncertainty analysis revealed that the uncertainty in the heat flux and the subcooling temperatures were nearly negligible for the purposes of this study with maximum uncertainties of 0.021 W and 0.14 °C respectively.

In order to estimate the uncertainty of the slug position analysis, the effect on the position of the filters used for the image processing was measured. A sequential perturbation method was used to calculate the uncertainty associated with using color threshold parameters to binarize the image. The color threshold parameters were varied for a frame of video. The position data was then determined for three slugs in the frame using the different color threshold parameters. The uncertainty was calculated from the root sum of the differences in position for each of the perturbation stages. Figure 18 shows the difference between the perturbed images using the different color threshold parameters. It was determined that this error was very small (around 7 microns). Due to the small error, the effect of binarization was determined to be negligible.

Figure 18: Sequential perturbation of color threshold parameters for binarizing the image for processing. a.) All parameters set at 10. b.) All parameters set at 250. This represents the start (a.) and end (b.) of the sequential perturbation analysis

Another possible source of error during the analysis was the inner edge being used, instead of the outer edge due to binary inversion step of the image processing. To measure this uncertainty, a sequential perturbation method was used. The difference in position value before and after binary inversion step was measured. Then the uncertainty from this process was estimated to be the root sum square of the uncertainty between

positions. Through this analysis was determined that the maximum uncertainty in the centroid position was about 1.6 pixels or around 0.0945 mm. The total error, assuming the error of time step is very small, in the velocity was calculated based on the equation:

$$u_v = \left(2\left(\frac{1}{dt}u_p\right)^2\right)^{\frac{1}{2}} \tag{12}$$

7. Results and Discussion

This sections overviews the collected data and discusses the results of the experiments. It is divided up by the geometry of the channel for comparison of the effects. The first subsection presents and discusses the observations and the qualitative results from the capture video. The second subsection discusses the quantitative results of the image analysis.

7.1. *Ratchets with Flat Sections*

This section looks at comparing the effects of flat geometries on the behavior of the bubbles. The first subsection looks at qualitative video and observations to classify the behavior. The second subsection discusses the results of image processing and numerical analysis.

7.1.1. Observations and Video Results

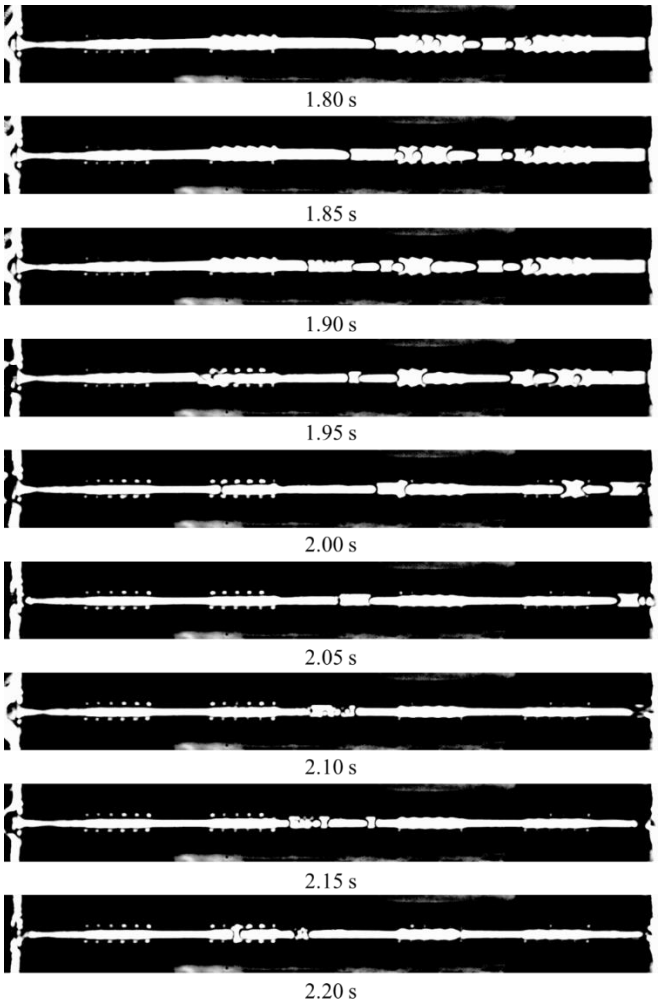

Figure 19: Video still from test with part flat geometry. The heat flux input was 0.4613 W/cm^2 with a subcooling of 2.67 °C.

Figure 19 shows bubbles that appear to form at the edges of the ratcheted sections and then form slugs that travel along the length of the channel. These slugs often travel along the direction of the ratchet. However, if a bubble is formed on the opposite side of the channel the flow of the bubble reverses. Several times during the tests the direction of the bubble was reversed, but the overall direction was generally in the preferential direction. This may occur because the partial flat geometries are smaller in width than the ratchet

sections. This causes the bubbles to contract during these sections, which can lead to barriers to bubble motion.

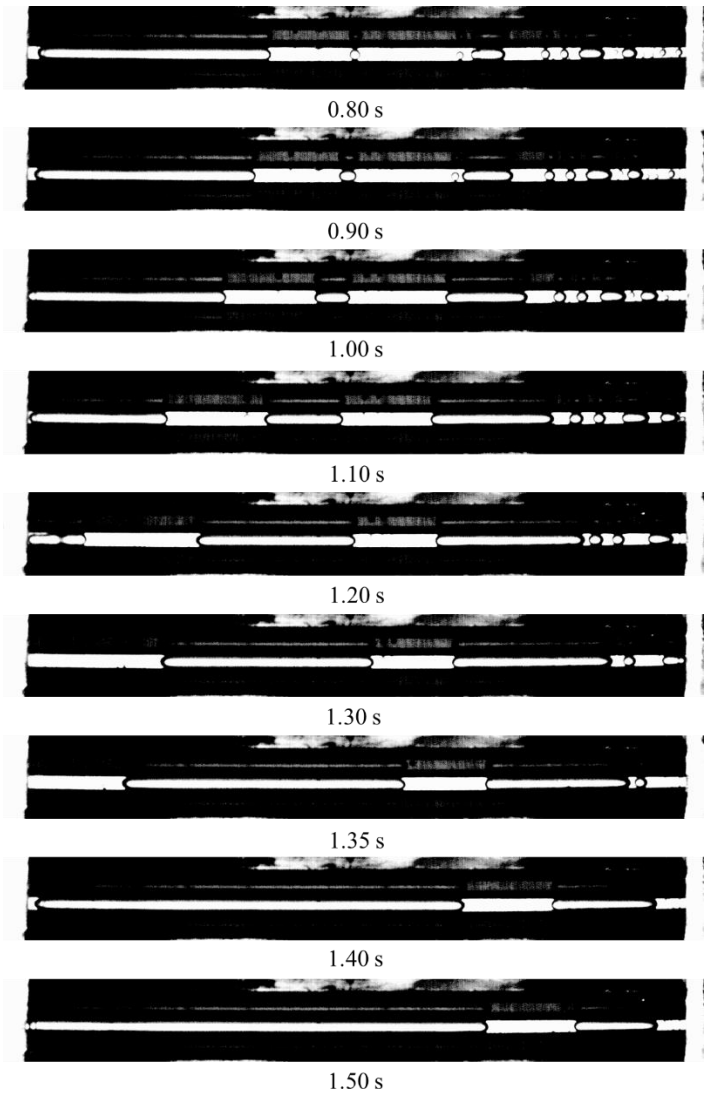

Figure 20: Video stills from test using flat surfaces. The test was run with a heat input of 0.44 W/cm^2 and a subcooling of 9.2 °C

Figure 20 shows a series of video stills from a test with partially flat geometry. The flat sections form smooth slugs that expand and vent outside the channel. The bubbles travel in both directions. Flat section behavior is much smoother than the asymmetric geometry.

7.1.2. Image Analysis Results

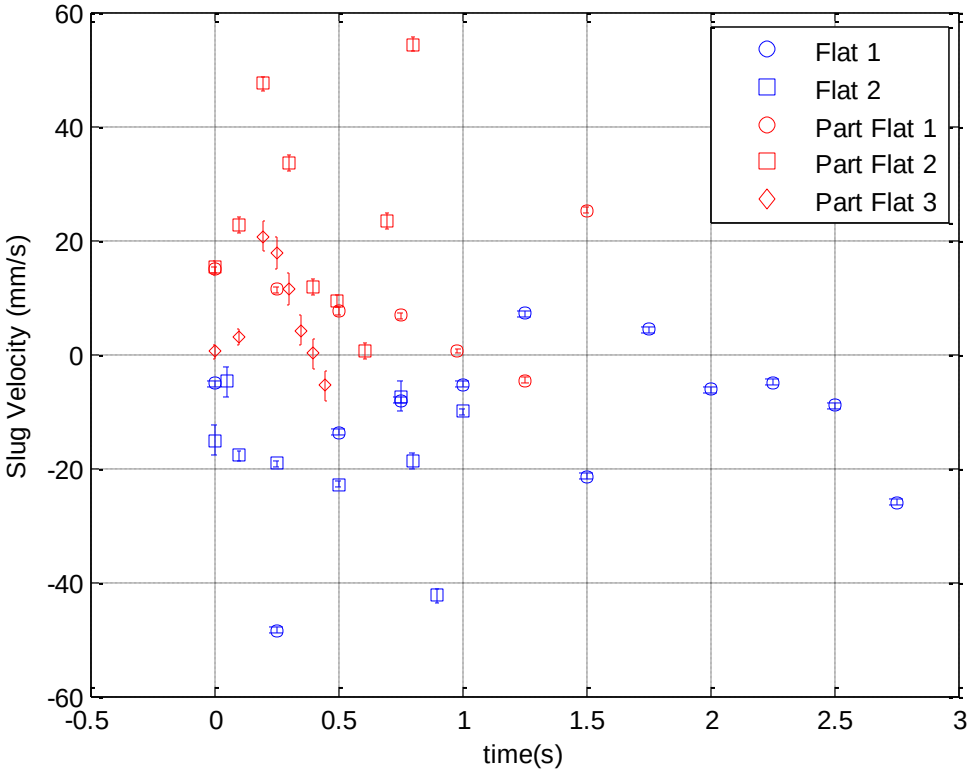

Figure 21: Center of mass velocity for different slugs comparing a surface with partially flat geometry (0.2306 W/cm^2 input and 4.54 °C subcooling) to a channel with fully flat geometry (0.296 W/cm^2 input and 4.1 °C subcooling)

There appears not to be much of a difference between the speeds of the center of mass between the partially flat and fully flat geometries besides the directions. The fully flat geometry was observed to have no preferential direction, while the partially flat geometry had a slight preferential direction. The velocity variation is most likely due to the influence of other bubbles. For the partially flat geometry, this variation could also be due to the changes in width of the channel. The flat sections contract due to the flat section being on plane with the peak of the ratchet, which accelerates the bubble through the section. The data shown in Figure 21 shows these spikes correspond to when the bubbles

are in the flat region. This can be shown in the video stills. The slugs tend to take less time to travel across the flat sections than the ratcheted section.

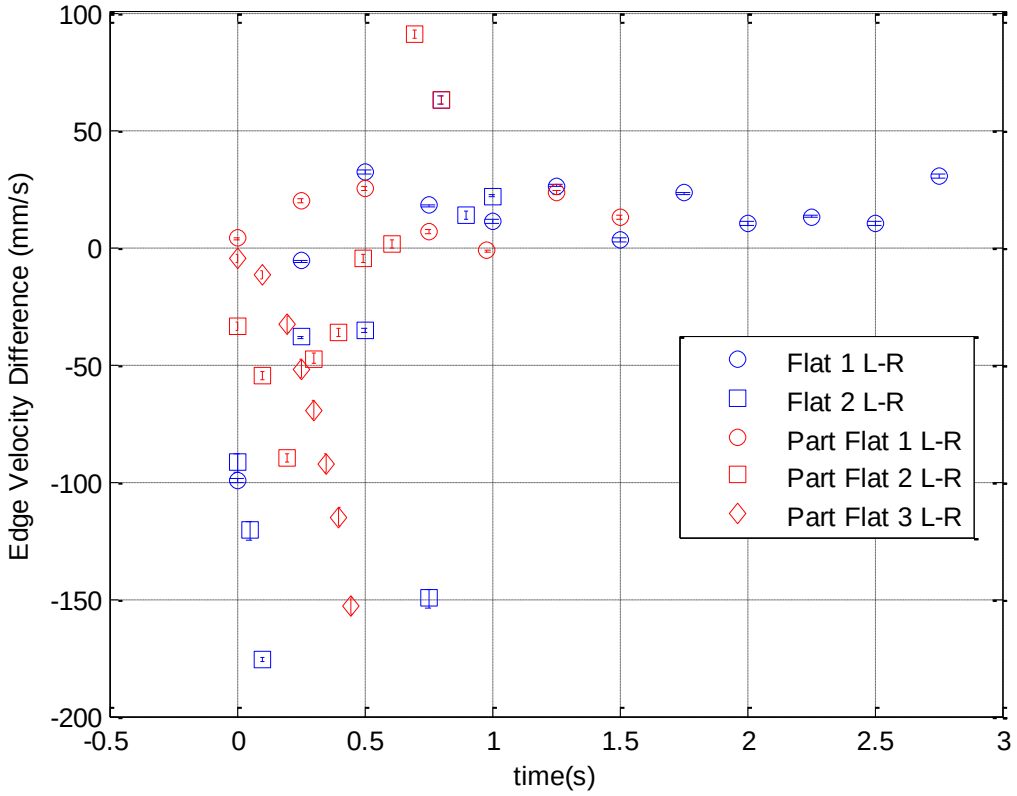

Figure 22: left and right edge velocity difference for several slugs comparing a surface with partially flat geometry (0.2306 W/cm^2 input and 4.54 °C subcooling) to a channel with fully flat geometry (0.296 W/cm^2 input and 4.1 °C subcooling)

Figure 22 shows the edge velocity difference for a ratchet with partially flat geometry and a ratchet with fully flat geometry. Slug 3 for the partially flat geometry shows rapid growth of both the left and right sides. Slug 2 shows large variations in the edge velocities, with growth mainly of the right side in the positive direction. This is most likely due the partially flat regions causing acceleration due to the contraction. Slug one shows mostly translational movement with slight retractions, as the left side is traveling faster to the right than the right side.

The flat geometry shows expansion of the slugs in the beginning. The slugs then move more towards translational movement and slight retractions. The movements toward translational motion may be mainly due to the buckled test section creating a barrier to growth on the right side. Before this, the fully flat geometry does show fairly even expansion of both sides.

Overall, the partially flat geometry exhibits more preferential to the right side, due to the asymmetric structures; while the fully flat geometry shows more even growth and less preferential direction.

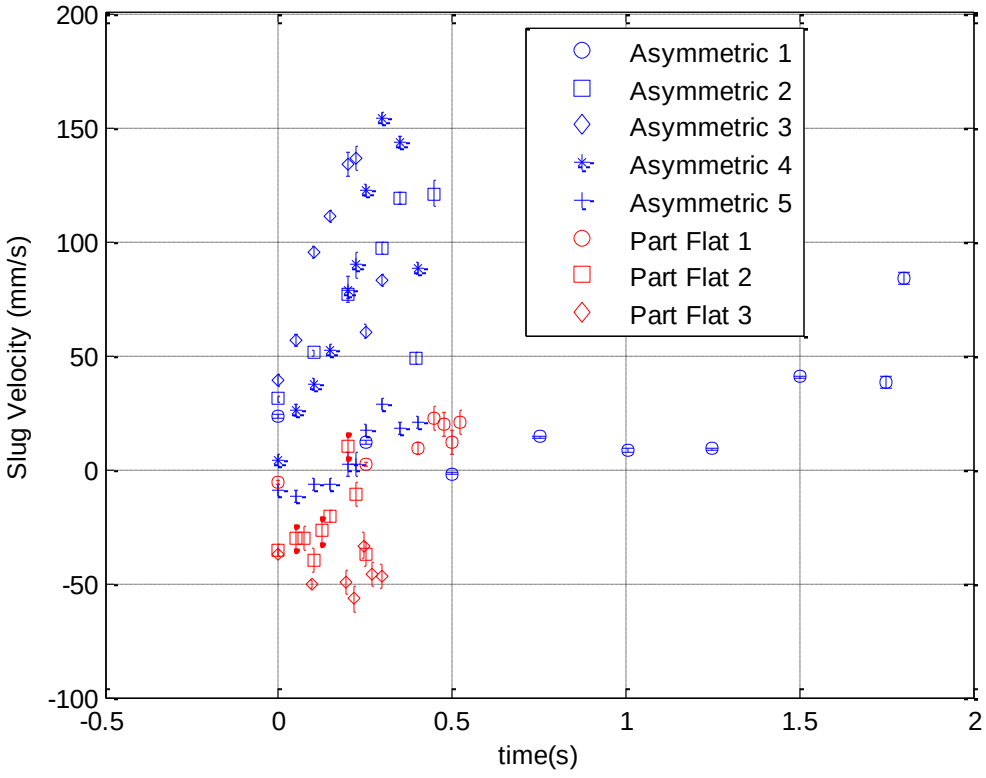

Figure 23: Center of mass velocity for different slugs comparing a surface with asymmetric geometry (0.258 W/cm^2 input and 0.82 °C subcooling) to a channel with partially flat geometry (0.1153 W/cm^2 input and 0.98 °C subcooling)

Figure 23 shows, the asymmetric ratchet appears to have a higher average velocity than the partially flat geometry. This is mainly due to the different behavior of the tests compared. For the asymmetric test, there are many small bubbles that are formed and expand before combining into large slugs. The part flat geometry showed large slugs that were fed by a few bubbles that quickly combined into the slug. Smaller bubbles tend to have larger speeds due being pulled by the large slugs during venting. Both tests show a preferential direction of the slugs in the direction of the shallow face that agrees with the previous tests. This is the negative direction for the part flat and the positive direction for the asymmetric case due to the tests being set up with the shallow angle in opposite directions of the video.

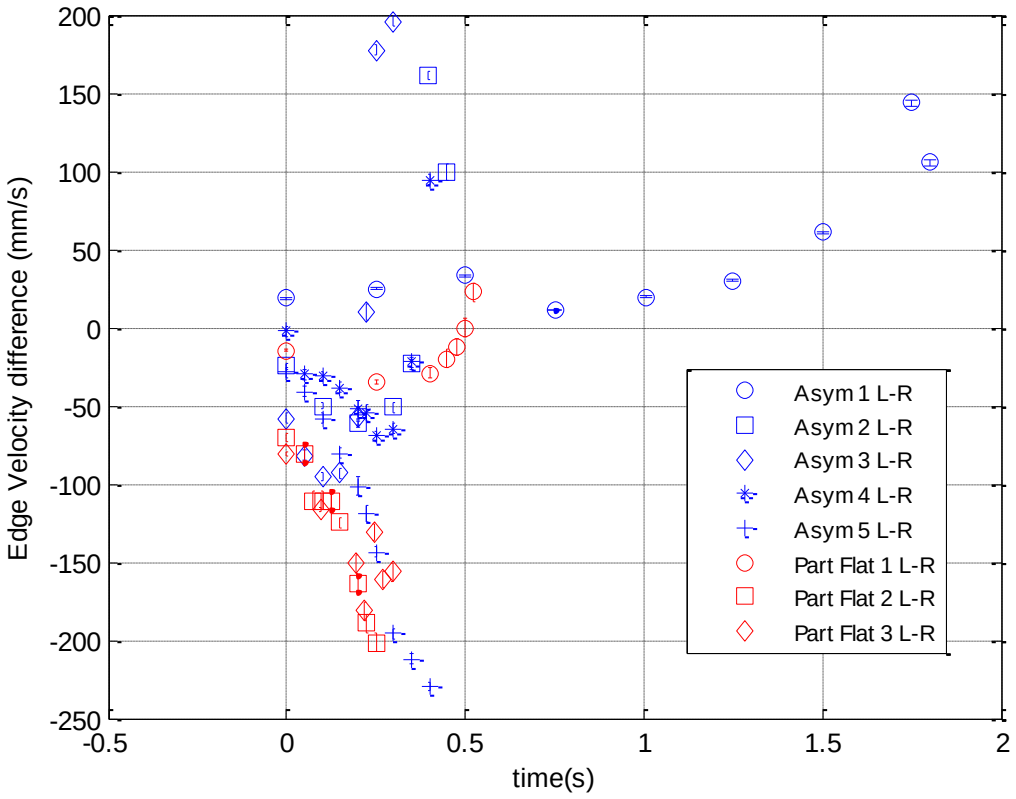

Figure 24: Difference between left and right edge velocity for different slugs comparing a surface with asymmetric geometry (0.258 W/cm^2 input and 0.82 °C subcooling) to a channel with partially flat geometry (0.116 W/cm^2 input and 0.98 °C subcooling)

The data in Figure 24 shows the difference between the lift and right sides of several slugs to help visualize the growth of the slugs. The asymmetric case show a large variation in slug growth. This is most likely due to the many small slugs that are formed in this case. These slugs are influenced by other slugs differently which manifests itself in the growth behaviors. Slugs 4 and 5 show fairly rapid expansion. These slugs show more rapid expansion of the right side as evidenced by the center of mass dat being mainly in the preferential direction. Slugs 2 and 3 show rapid growth, then deceleration followed by retraction. This is due to these slugs expanding to the right and then the left side

retracting as the slug vents. Slug 1 shows mainly translational motion toward the beginning, then retraction of the slug.

For the partially flat geometry, most of the slugs show growth. Slugs 2 and 3 show rapid acceleration of growth. These slugs show rapid growth of both sides, but overall slightly faster growth of the left side. This shows a slight preferential direction for these slugs. Slug 1 shows initial growth, but then deceleration and retraction. This is due to this slug expanding and then venting outside the channel.

Overall, the asymmetric geometry shows a stronger preferential direction than the partially flat geometry. The partially flat geometry exhibits more even growth of the slugs, while the asymmetric case shows mush more rapid growth of the edge in the preferential direction.

The event analysis case for comparing asymmetric structures to partially flat looked at a test with partially flat geometry with a heat input of 0.92 W/cm^2 and a subcooling of 2.35°C and a test with asymmetric geometry and 0.92 W/cm^2 and a subcooling of 2.63°C. The results showed 0 venting events in the typical preferential direction and 459 events in the opposite direction for the part flat geometry. The asymmetric geometry showed 116 in the typical preferential direction and 27 in the opposite direction. These results show that the part flat case was more active, however showed all of the activity opposite of the desired preferential direction. This shows a case where the flow reversed for the partially flat geometry. This was observed a couple times during testing. It is believed that the partially flat sections can create a barrier to bubble growth at certain points in the

channel. This forces the flow to reverse if a bubble starts growing on the opposite end of the channel and then vents thereby creating a favorable pressure gradient.

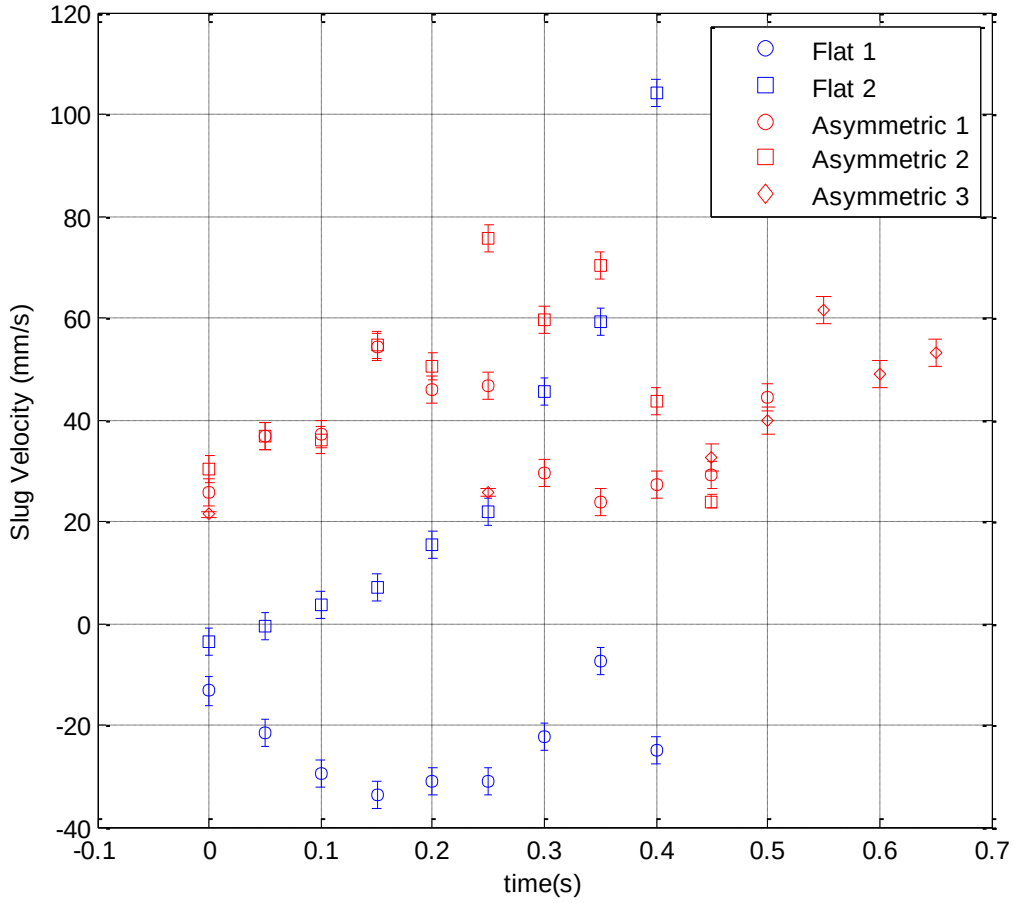

Figure 25: Center of mass velocity for different slugs comparing a surface with asymmetric geometry (0.515 W/cm^2 input and 8.96 °C subcooling) to a channel with flat geometry (0.44 W/cm^2 input and 9.2 °C subcooling)

The velocities in Figure 25 show no preferential direction for the flat case. Each slug travels in a different direction. The asymmetric slugs show a distinct preferential direction in the velocity data. The flat case shows a higher peak velocity, but the asymmetric case shows a higher consistent velocity.

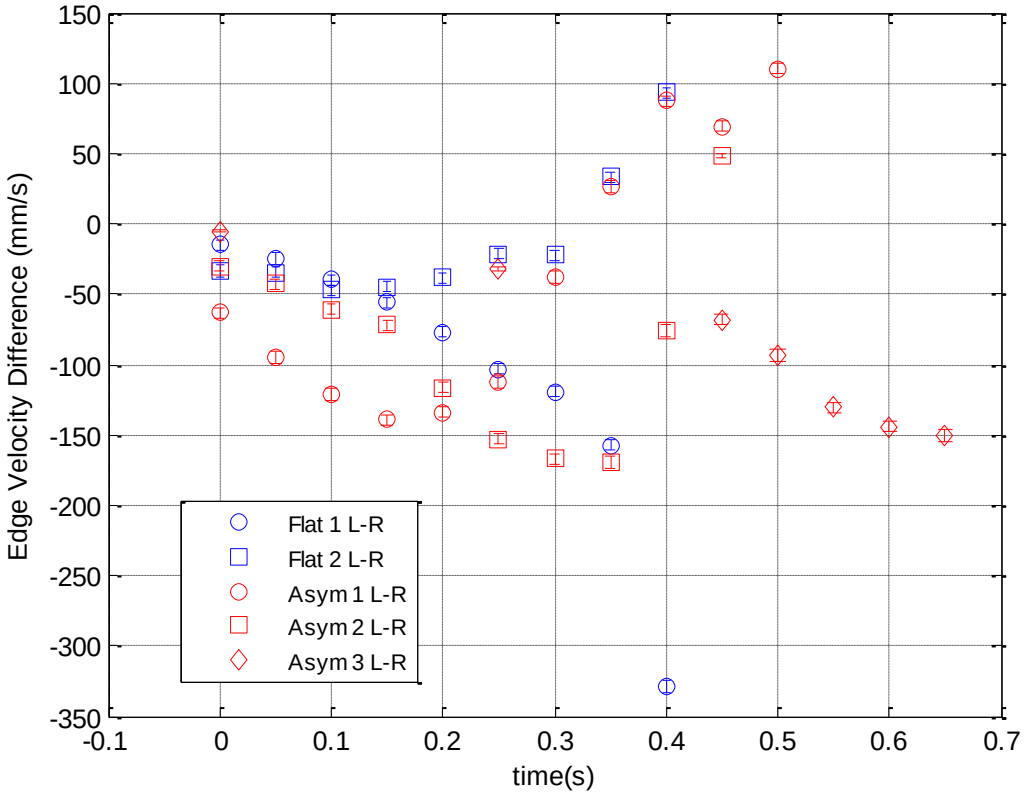

Figure 26: Left and right edge velocity difference for several slugs comparing a surface with asymmetric geometry (0.515 W/cm^2 input and 8.96 °C subcooling) to a channel with flat geometry (0.44 W/cm^2 input and 9.2 °C subcooling)

The edge velocity in Figure 26 presents the growth rate of several slugs for the asymmetric and fully flat cases. The asymmetric geometry shows most slugs expanding fairly rapidly. These slugs show faster edge velocities in the preferential direction. Some slugs show contraction. This contraction is due to the slugs reach one end of the channel and venting into the pool. The venting and contraction is in the preferential direction for this case.

The flat geometry shows one slug expanding and one slug contracting. This is due mainly to the type of slugs that were captured. The slug contracting is venting to one side of the channel. This is due to the slug being formed on one side of the channel, then expanding

until it reaches the edge of the channel, then vents and contracts. For slug 1, the data shows fairly even expansion for both the left and right side in opposite directions. This shows a lack of preferential direction in the flat case. The flat geometry allows for more even expansion.

Overall the growth data supports the center of mass data and data from other plots. The asymmetric case shows a strong preferential direction, while the flat section shows little to no preferential direction.

7.2. *Symmetric Ratchets*

This section looks at comparing the effects of symmetric ratchets on the behavior of the bubbles. The first subsection looks at qualitative video and observations to classify the behavior. The second subsection discusses the results of image processing and numerical analysis.

7.2.1. Observations and Video Results

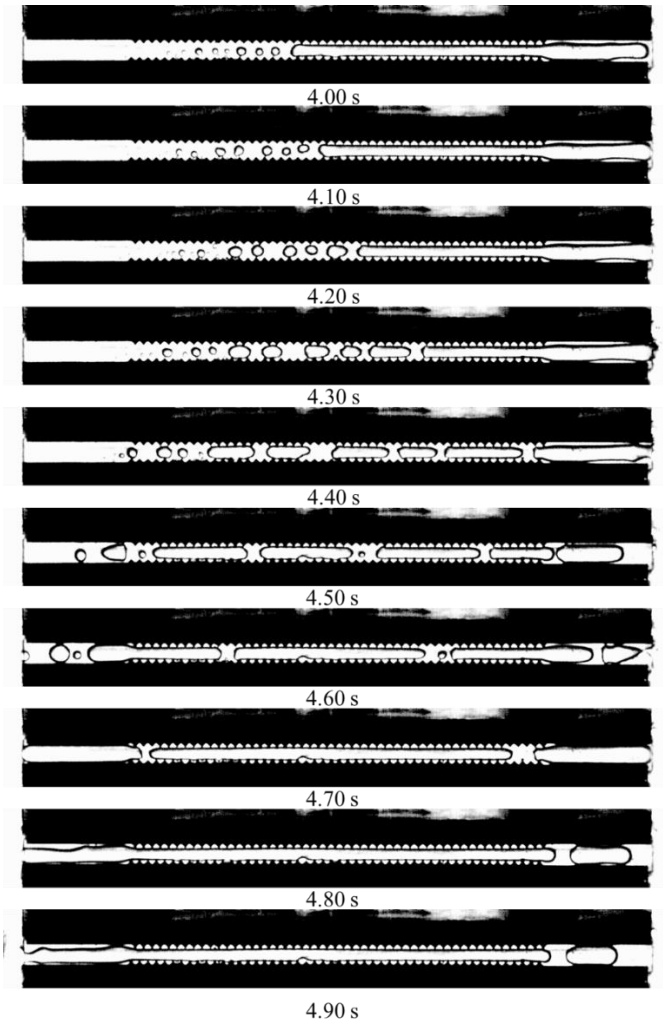

Figure 27: Video still from a test with a symmetric ratchet structure offset by one half of the pitch. The heat flux input was 0.713 W/cm^2 with a subcooling of 2.27 °C

The symmetric case shows no preferential direction. The bubbles often expand towards whichever side is closer. This causes venting out both sides to occur during the test. The flow and expansion of bubbles appears much more chaotic than for other tests. As with most cases, the influence of other bubbles was observed to drive the flow also.

7.2.2. Image Analysis Results

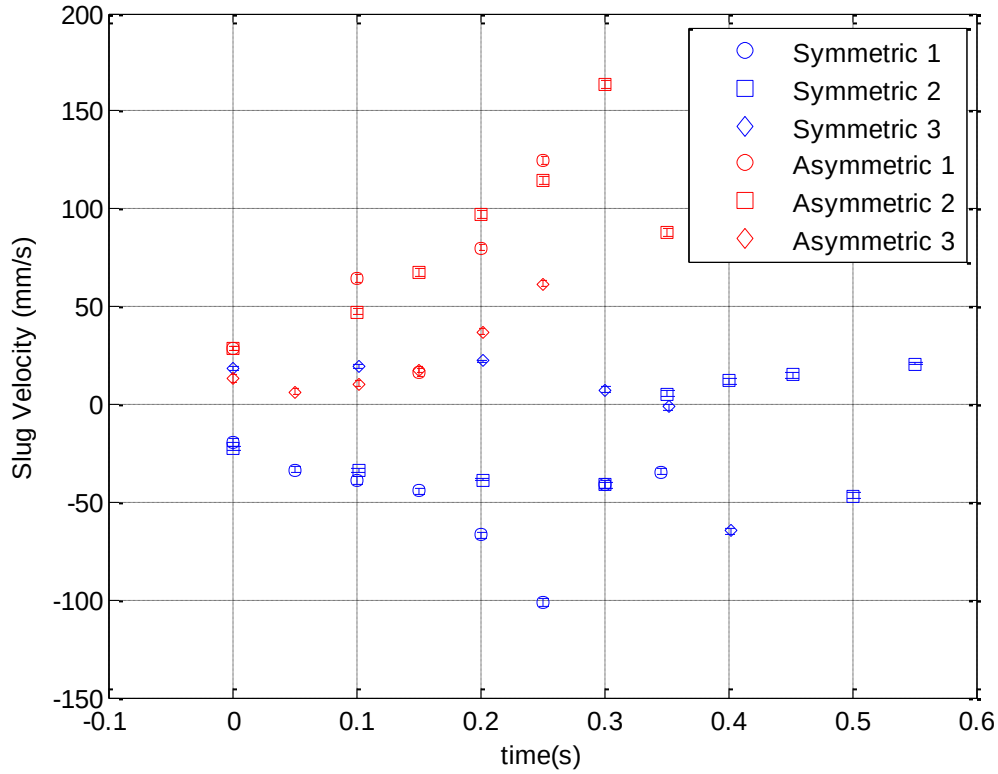

Figure 28: Center of mass velocity for different slugs comparing a surface with asymmetric geometry (0.92 W/cm^2 input and 2.64 °C subcooling) to surface with symmetric geometry (0.713 W/cm^2 input and 2.27 °C subcooling)

The velocity data presented Figure 28 shows faster velocities and larger accelerations for the asymmetric case than the symmetric case. It also shows less of a preferential direction for the symmetric case. The slug velocity for the asymmetric case are only in the positive direction, while for the symmetrical case the velocities are in both the positive and negative directions.

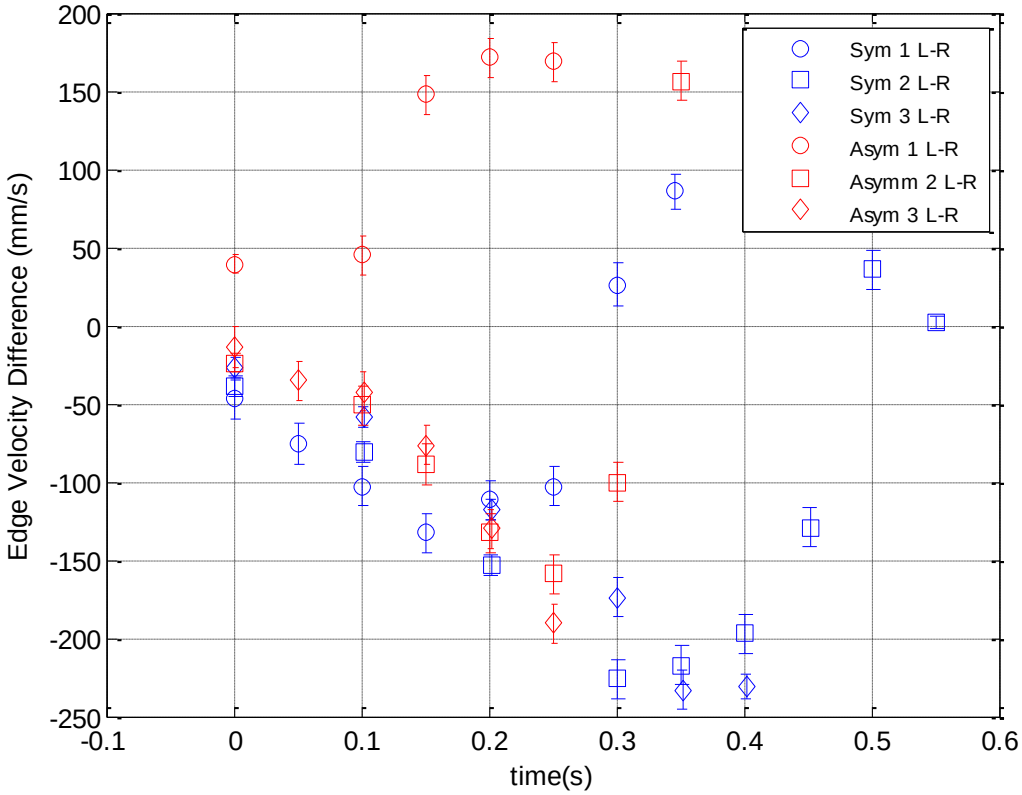

Figure 29: Left and right edge velocity difference for several slugs comparing a surface with asymmetric geometry (0.912 W/cm^2 input and 2.64 °C subcooling) to surface with symmetric geometry (0.713 W/cm^2 input and 2.27 °C subcooling)

The growth velocity data in Figure 29 shows similar behaviors for both cases. Both geometries show dome slugs that expand and others that contract. It is difficult to comment on the behavior unless the center of mass data is considered also.

The asymmetric case shows a more distinct direction. Most of the expansion is in the preferential direction with very little expansion of the left side. Most of the movement of the left side is in the right direction. This shows very strong preferential direction. The symmetric case shows much more similar velocities for the left and right cases. This is reflected in the center of mass data. The center of mass velocity is lower for the

symmetric case due to this fairly even expansion. Symmetric ratchets show less preferential direction than the asymmetric ratchets for these conditions.

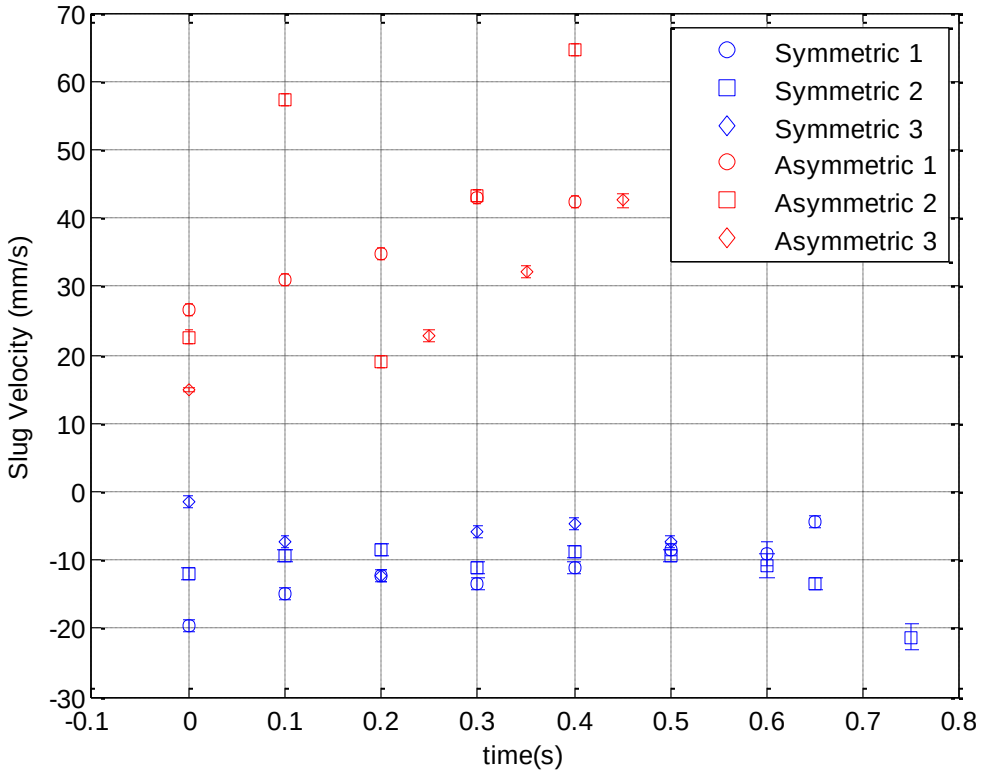

Figure 30: Center of mass velocity for different slugs comparing a surface with asymmetric geometry (0.13 W/cm^2 input and 2.38 °C subcooling) to surface with symmetric geometry (0.05 W/cm^2 input and 2.06 °C subcooling)

The data in Figure 30 shows much higher velocities for the asymmetric case than the symmetric case. It also shows more acceleration in the asymmetric case. The symmetric case has a more consistent average velocity. Both velocities show values in one direction. In the symmetric case this is mainly due to bubbles forming at the left end, expanding and venting out the left end.

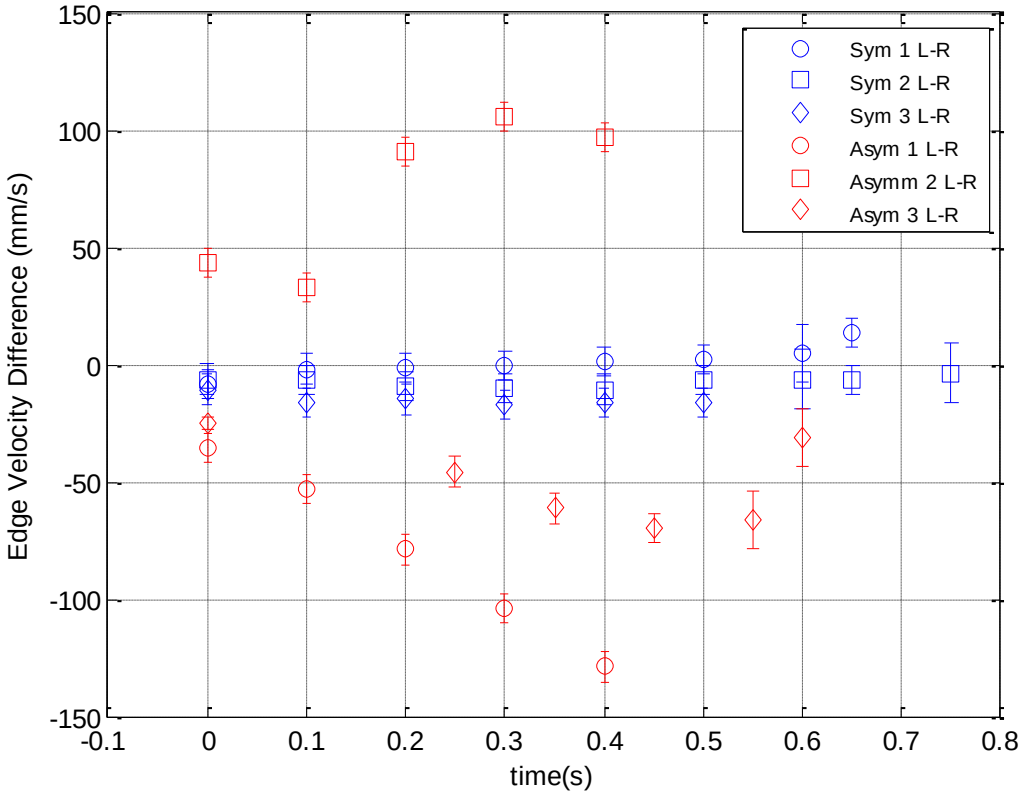

Figure 31: Left edge and right edge velocity difference for several slugs comparing a surface with asymmetric geometry (0.129 W/cm^2 input and 2.38 °C subcooling) to surface with symmetric geometry (0.05 W/cm^2 input and 2.06 °C subcooling)

The symmetric case shows fairly consistent growth velocities for the edge velocity data in Figure 31. These values are also generally centered around zero. This shows a tendency for the slugs to have more translational motion instead of growth in one or both directions when compared with the center of mass data. The asymmetric case shows much more varied motion of the bubbles. Some slugs grow, while one is retracting. This is mainly due to the different behavior of the slugs at different locations. The slug that is retracting is at the edge of the channel and venting into the pool. The expanding slugs are in the middle of the channel and growing outward. These slugs show most of the expansion in the preferential direction for the asymmetric case.

Overall the asymmetric case shows more of a preferential direction than the symmetric case for this test state. Another major distinction between the cases is the velocities observed. The asymmetric case shows large velocities with peaks around 150 mm/s for the growth of several slugs. While the symmetric case has much lower velocities. This is due to the behavior of the slugs. The symmetric case has bubbles that formed on the left edge expand and then vents to the left edge. This explains why the right edge velocity is slightly lower than the left edge.

7.3. *Channel Width*

This section looks at comparing the effects of channel width on the behavior of the bubbles. The first subsection looks at qualitative video and observations to classify the behavior. The second subsection discusses the results of image processing and numerical analysis.

7.3.1. Observations and Video Results

This section presents and discusses video results from tests to compare different channel width geometry. Figure 32 shows a series of video stills from a test with a channel width of 1 mm with a heat flux input of 1.116 W/cm^2 and a subcooling of 11.9 °C. Figure 33 presents stills from a test with a channel width 1.5mm with a heat flux input 0.99 W/cm^2 and 12.45° C of subcooling in the pool.

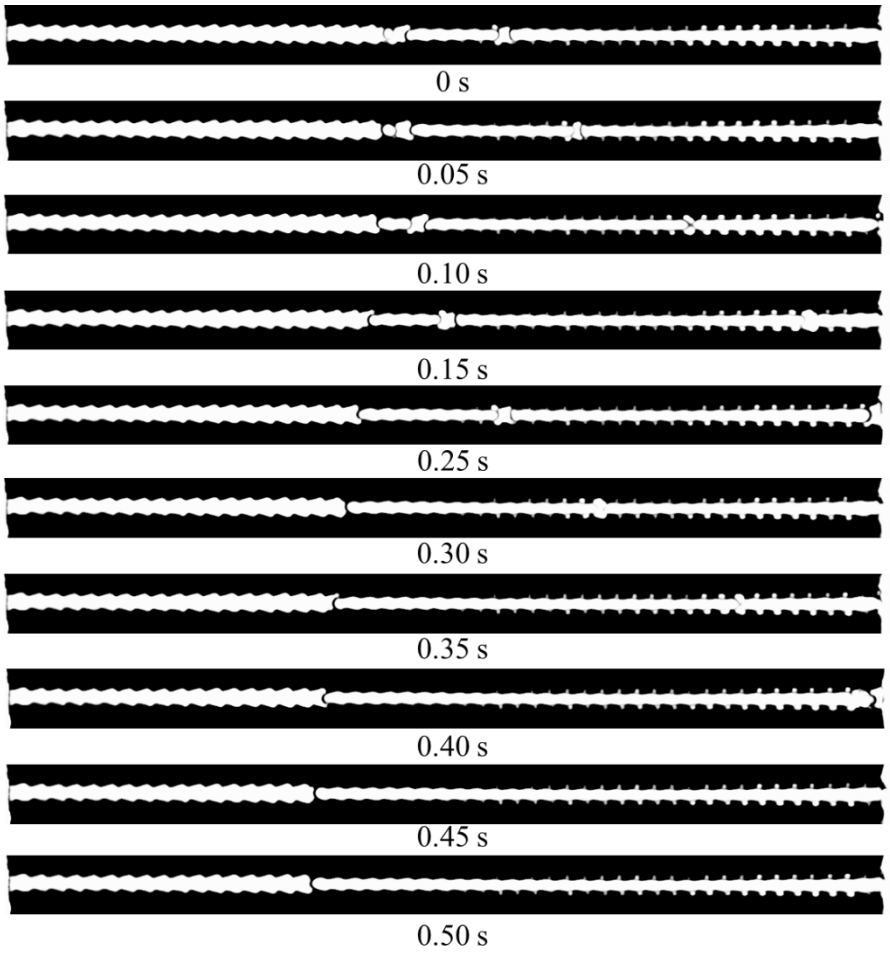

Figure 32: Video stills for a channel with 1 mm width. The inputted heat flux was 1.03 W/cm^2 with a subcooling of 11.9 °C

The video stills in Figure 32 show small slugs forming which quickly coalesce into one giant slug. The slug grows to the left due to the merging of slugs. However the slug is venting to the right which corresponds to the direction of less steep side of the ratchet. This agrees with past experiments.

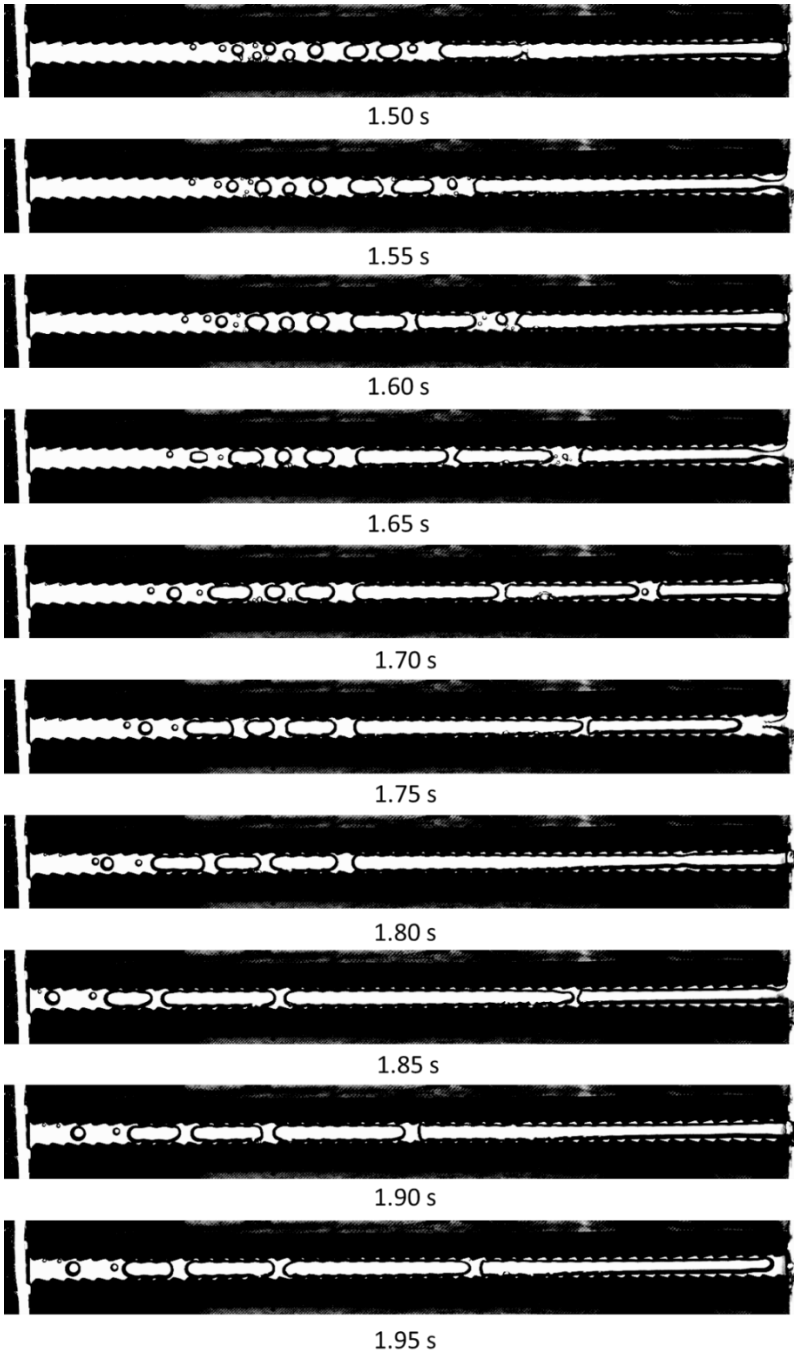

Figure 33: Video stills from a test with a channel width of 1.5 mm. The heat input was 0.92 W/cm^2 with 12.45° C of subcooling in the pool

Figure 33 shows several small slugs forming in the channel. These slugs travel expand, then combine and vent to the right. Smaller bubbles feed and coalesce into larger slugs to continue the growth.

Both Figure 32 and Figure 33 show a preferential bubble direction consistent with previous results. The bubble travel along the channel in the direction that corresponds to the side with the less steep surface angle. The major difference between the observed behaviors between the two tests was that the 1.5 mm channel width produced more observable bubbles, while the 1 mm ratchet tended to produced single large slugs for similar heat flux inputs. This is most likely due to there being less fluid inside the 1 mm channel. The fluid turns to vapor quickly and produces a single large slug. Vice versa, the 1.5 mm channel has more fluid and which allows more time for single bubbles to form and grow before they coalesce into one large slug.

7.3.2. Image Analysis Results

This subsection presents the results of the image processing used for comparing the effect of channel width on the behavior of the bubbles. Figure 34 shows the center of mass velocity for several slugs tracked for both the 1.5 mm and 1 mm tests. Figure 35 shows the left edge and right edge velocities for several slugs tracked for both the 1.5 mm and 1 mm tests.

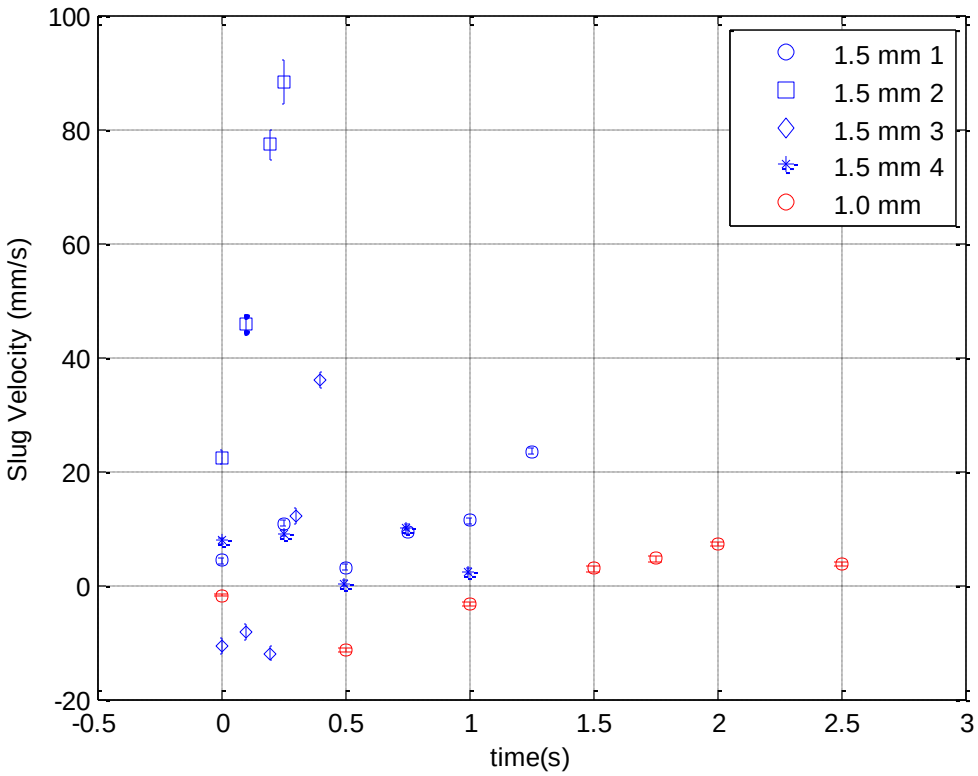

Figure 34: Center of mass velocity for different slugs comparing a channel width of 1 mm (1.03 W/cm^2 input and 11.9 °C subcooling) to a channel with width of 1.5 mm (0.92 W/cm^2 input and 12.45 °C subcooling)

The 1 mm channel width starts off traveling in the negative direction because the slug is expanding while venting during the tracking period, which shifts the center of mass in the negative direction. It then travels in the positive direction as it continues to vent and the slug contracts. Only one slug was formed during this test was easy to track for this test, due to the small amount of fluid quickly converting to vapor. The slugs for the 1.5 mm channel have much more variability. This is mainly due to many slugs of different sizes. These slugs expand at different rates and are influenced by each other, which shows up as variance in the velocities.

Overall it appears that the 1.5 mm channel width has larger bubble velocity, but this is possibly due to the smaller bubbles that are formed in the 1.5 mm channel. These bubbles are accelerated by the large slugs venting. This creates large velocities in the small bubbles.

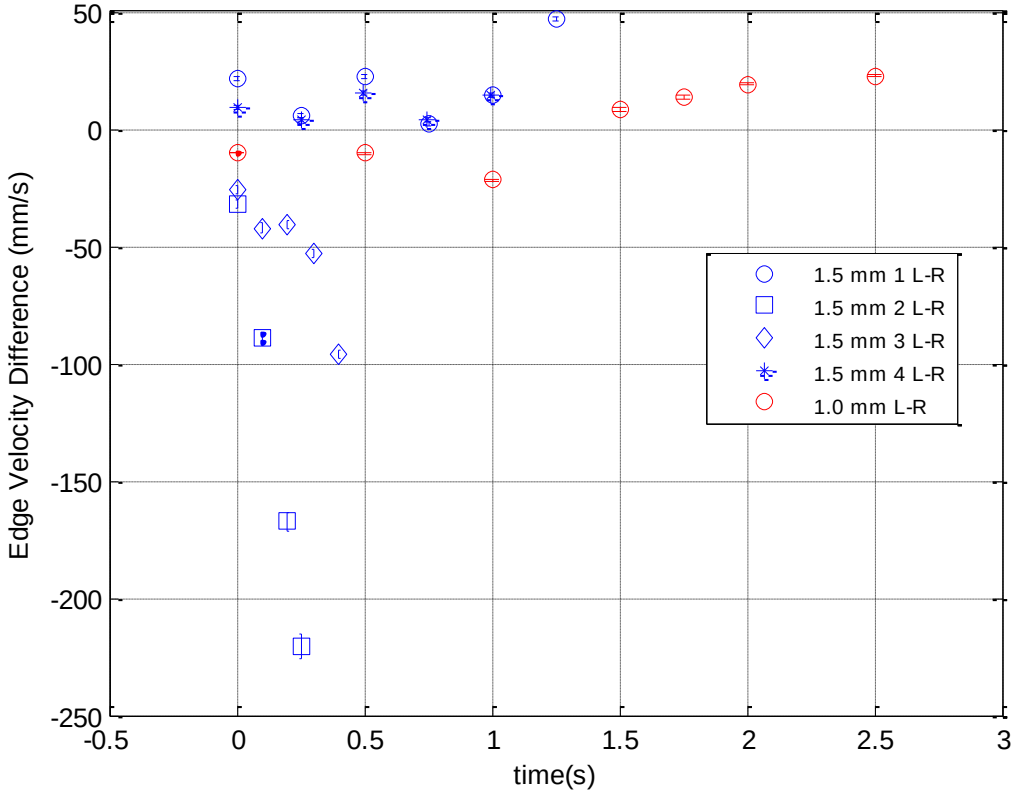

Figure 35: The left and right edge velocity difference for several slugs comparing a channel width of 1 mm (1.03 W/cm^2 input and 11.9 °C subcooling) to a channel with width of 1.5 mm (0.92 W/cm^2 input and 12.45 °C subcooling)

Figure 35 shows that the left side of the slug in the 1 mm channel begins expanding to the left and then retracts as the bubble vents out the channel. This corresponds with the center of mass data. The growth of this slug is almost completely influenced by the left edge velocity. The right edge is very near zero. The shows that the slug is venting in the preferential direction for this channel.

The 1.5 mm channel shows slugs that expand and slugs that retract. This is due to the behavior of slugs at different points in the channel. For the expanding slugs, the most of the growth is in the preferential direction. The retracting slugs show similar movements in the preferential direction, as evident by the center of mass data.

Overall, both channel widths show preferential directions similar to previous tests for the asymmetric case. The 1 mm channel tends to form one slug that vents due to having much less fluid inside the channel. The 1.5 mm channel forms several slugs that influence each other and travel in the preferential direction.

The event data for the 1.5 mm channel with a 2.06 W/cm^2 heat input revealed that 132 venting events occurred to the right and 0 events to the left. The event data for the 1.0 mm channel with a 2.06 W/cm^2 heat input revealed that 162 venting events occurred to the right and 51 events to the left. This shows preferential direction to the right for both cases, which is consistent with other data. This data also suggest that the 1 mm channel is more active on both sides at a similar heat input than the 1.5 mm channel. This is due to the smaller amount of fluid in the channel forming more vapor, faster.

7.4. *Offset Ratchets*

This section looks at comparing the effects of offsetting the ratchets by half a pitch on the behavior of the bubbles. The first subsection looks at qualitative video and observations to classify the behavior. The second subsection discusses the results of image processing and numerical analysis.

7.4.1. Observations and Video Results

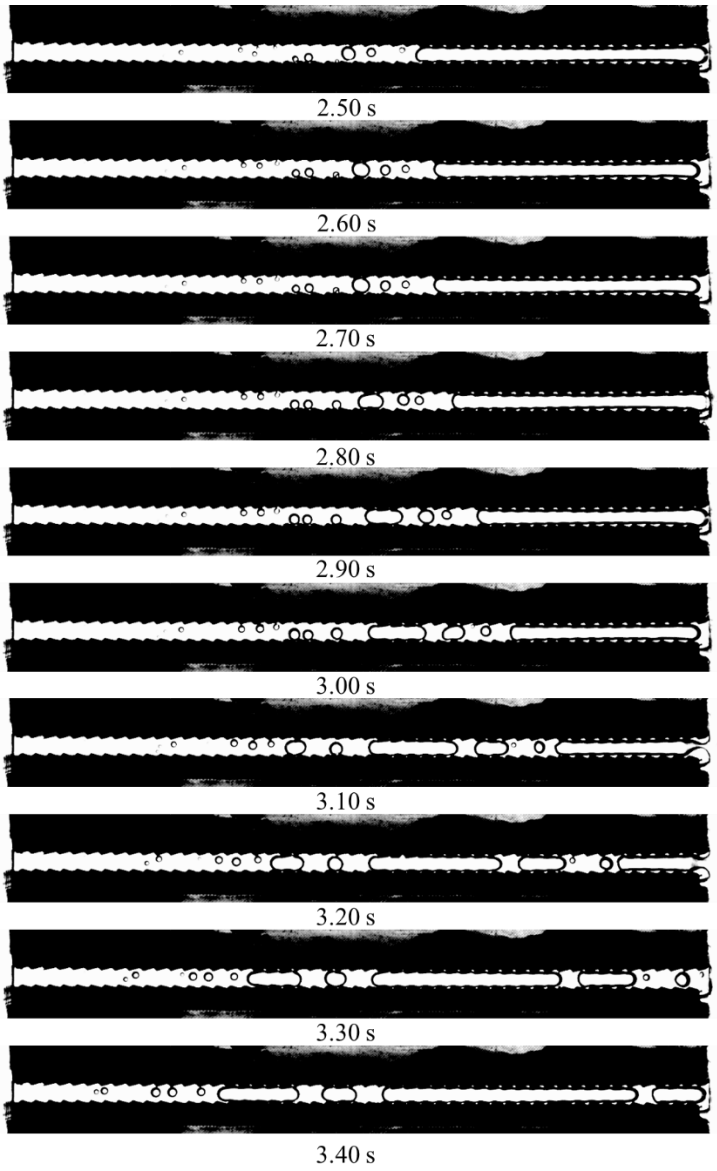

Figure 36: Video still from a test with an asymmetric ratchet surface offset by one half of the pitch. The heat flux input was 0.92 W/cm^2 with a subcooling of 2.64 °C

Figure 36 shows video stills from a test with asymmetric ratchets offset by one half the ratchet pitch. The offset case shows similar behavior to the normal case. There is a preferential direction for the growth and venting of the bubbles. One observation was that the motion of the leading and trailing is clearly in an up and down motion. This is due to

the ratchet geometry. In the non-offset case this leads to local expansion and contraction. Figure 37 shows a detailed view from two video stills that illustrate the up and down motion of the trailing edge.

Figure 37: Detailed view of subsequent video stills showing the up and down motion of the trailing edge due to the peaks and troughs of the ratchets alternating

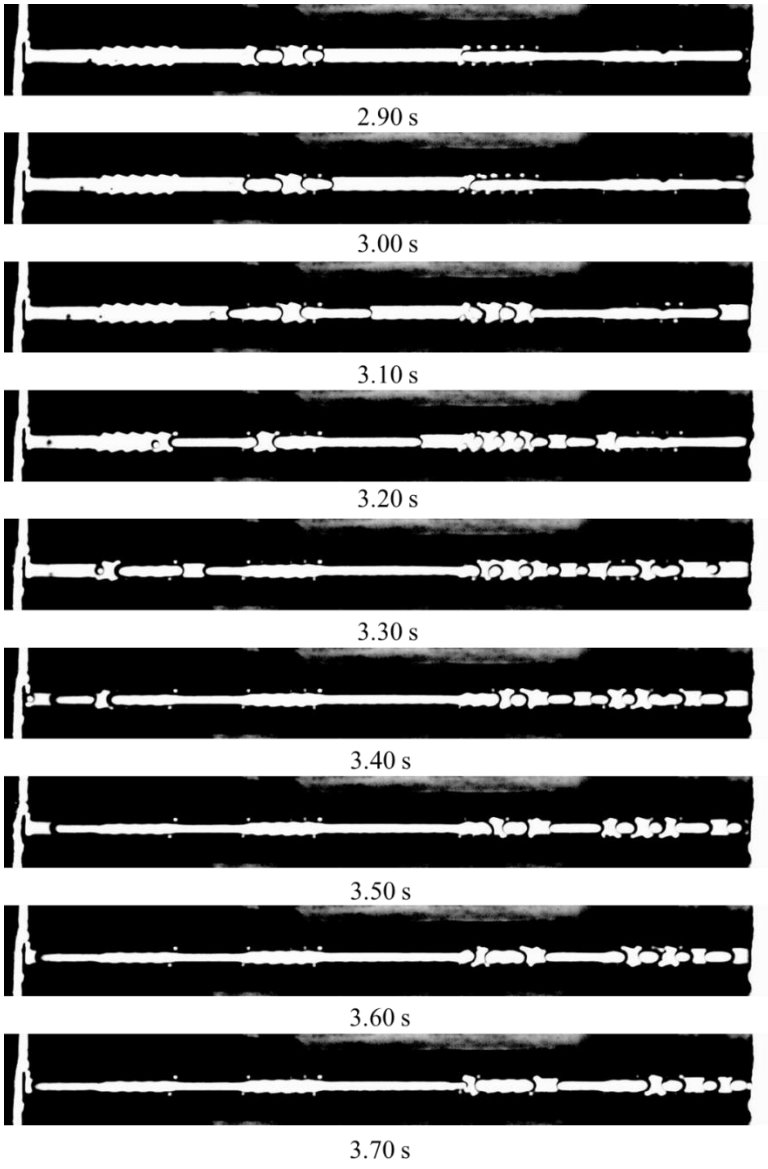

Figure 38: Video still from a test with a partially flat ratchet surface offset by one half of the pitch. The heat flux input was 0.23 W/cm^2 with a subcooling of 4.54 °C

The offset case shows similar behavior to the non-offset case for partially flat geometry. There is local contraction through the flat sections. There appears to be a bit more of a tendency for the bubbles to reverse direction than in the non-offset case. Figure 38 shows the flow starting to reverse during the test starting around 3.2 seconds. This may be due to less of a local barrier to expansion of the bubble due to contraction of the channel.

7.4.2. Image Analysis Results

Table 3 shows the results of the venting analysis used to compare the effect of offsetting the ratchets for partially flat geometry. This analysis was chosen for both the tests because it was difficult to track individual bubble activity due to one large slug.

Table 4: Table of venting event analysis used to compare the effect of offsetting the ratchet for partially flat geometry.

Geometry	Offset		Non-offset	
q" (W/cm^2)	0.69	1.85	0.69	1.85
Subcooling (°C)	2.71	2.75	2.93	1.62
Events in Desired Preferential Direction	0	141	338	50
Events Opposite Desired Preferential Direction	85	4	51	174

The analysis shows that the non-offset geometry tends to be more active at similar input conditions than the offset case. This could be due to local expansion and contractions pushing the bubble along the channel, which exist for the non-offset case. The analysis also shows that both the offset and non-offset case can have the tendency to vent out the channel on the opposite side of the preferential direction. This phenomena is present in the lower heat flux input test. This could be due to the boiling being less active, causing less forcing toward the desired preferential direction.

8. Conclusions and Recommendations

Video and experimental observations were useful in observing the overall behavior of the bubbles. The slug velocities gave further insight into the direction of the bubbles in the channel and the event analysis script was useful for looking at the boiling behavior of the channel. Using these tools it was observed that geometric conditions can have an effect on the boiling behavior of an open-ended channel passive pump.

Decreasing the channel width tended to increase the amount of vapor and the slug size inside the channel for similar inputs. This lead to a decrease in slug velocity and an increase in boiling activity under similar conditions. It had little or no effect on the preferential direction of the bubbles. Adding flat geometry showed a decrease in the preferential direction of the test section. Sections with partial flat geometry showed a tendency to reverse direction more often and exhibited lower slug velocities. This could be explained by the contraction of the flat sections created barriers causing bubbles to be more likely to flow the in the direction of the edge they were formed on. Offsetting the geometry showed reductions in the local expansion and contraction of the bubbles due to the ratchets. The offset case also exhibited less venting activity under similar conditions. Symmetric ratchets showed almost no preferential direction. This case also showed slightly lower slug velocities. According to the trends excepted an ideal channel to increase boiling activity would include asymmetric ratchets with a thin channel.

From past work, there are two major driving forces of the bubble direction. The first is the pressure differences due the curvature of the bubbles and the second is local

expansion and contraction due to the troughs and peaks of the ratchet. The offset case showed less activity in the preferential direction than the non-offset case. This suggests that the local expansion and plays an important role in the open-ended channel configuration. It is not fully understood why the local expansions and contractions cause a preferential direction in the direction of the shallower ratchet slope. It may be due to a mixture of bubble momentum, the local curvature driving flow, and the acceleration through a sudden contraction. Figure 39 shows an illustration of the channel to be used in the discussion of the possible physics.

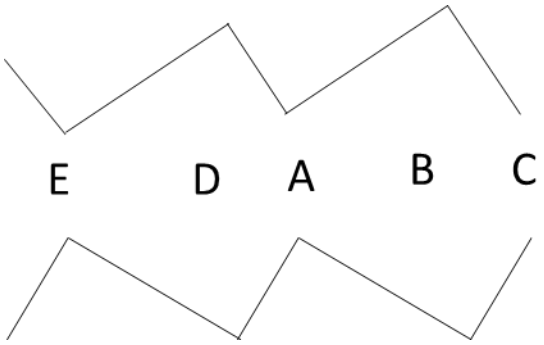

Figure 39: Diagram of channel with contractions and expansions labeled

Due to the local expansion a bubble forming at point A will want to expand to point D faster than to point B due to the sudden expansion of the channel. It will also expand to B, albeit more slowly. The bubble front on the left side will then slowly move from D to E due to the inertia of the front, while continuing to expand from A to B. Once it reaches B, the momentum may carry the bubble through the rapid contraction at C. This would cause rapid acceleration of the bubble as suggested by the results for partially flat geometry showing slugs accelerating through the flat section. The combination of momentum and these contractions could rapidly expand the slug to the right. The local

curvature would also contribute to the momentum of the bubbles. The left side may not have as rapid acceleration because the contraction is much more gradual on the shallow sides. In addition the mechanism proposed by Strid [3] would subtract from the momentum of the bubble, which may stop the bubble from expanding through these contractions. The data showed some cases where the edge of the slug was near stopped for the asymmetric case. This suggests that something is limiting the expansion. The combination of the two driving forces for bubble growth and the momentum of the bubble could explain the observed preferential direction.

It is difficult to comment on the effectiveness on the geometrical changes. The velocity of the slugs was collected but is mainly useful to observe overall trends and confirm the preferential direction. Faster slug velocities doesn't always translate into more boiling activity. There were a few cases that exhibited this behavior. Therefore another method should be developed to determine the effectiveness of the channel. One way would be to measure the circulation of the pool. This could be done with a Particle Image Velocimetry (PIV) system. These systems track seeder particles that have similar properties to the fluid by illuminating them with laser to obtain velocity fields of the fluid. Alternately, a simpler system of tracking neutrally buoyant particles could be used to obtain data.

Future experiments should look at more changes to the geometry of the channel. One candidate could be to look at the angle of the ratchet surface. Other channel widths could also be explored.

9. Bibliography

[1] 3M, "Fluorinert™ Electronic Liquid FC-72-Product Information," 2014. [Online]. Available: http://multimedia.3m.com/mws/mediawebserver?mwsId=66666UgxGCuNyXTtnxTE5XF6EVtQEcuZgVs6EVs6E666666--&fn=prodinfo_FC72.pdf. [Accessed 2014].

[2] F. Kapsenberg, "Lateral Fluid Motion in Nucleate Boiling Throug Asymmetric Surface Structures," Oregon State University, Corvallis, OR, 2011.

[3] L. Strid, "Passive Pumping in Pool and Open Channel Configurations via Meso-Scale Asymmetric Surface Patterning," Oregon State University, Corvallis, Oregon, 2013.

[4] H. Linke, B. J. Aleman, M. L. D, M. J. Taormina, M. J. Francis, C. C. Dow-Hygelund, V. Narayanan, R. P. Taylor and A. Stout, "Self Proppelled Leidenfrost Droplets," *Physical Review Letters*, no. 96, 2006.

[5] R. Feng, W. Zhoa, X. Wu and Q. Xue, "Ratchet composite thin film for low-temperature self-propelled Leidenfrost droplet," *Journal of Colloid and Interface Science,* no. 367, pp. 450-454, 2012.

[6] G. Lagubeau, M. L. Merrer and D. Quéré, "Leidenfrost on a ratchet," *Nature Physics*, no. NPHYS1925, 2011.

[7] N. Thiagarajan, F. Kapsenberg, V. Narayanan, S. H. Bhavnani and C. Ellis, "On the Lateral Motion of Bubbles Generated From Re-Entrant Cavities Located on Asymmetrically Structured Surfaces," in *Pacific Rim Technical Conference and Exhibition on Packaging and Integration of Electronic and Photonic Systems*, Portland, Oregon, 2011.

[8] F. Kapsenberg, L. Strid, N. Thiagarajan, V. Narayanan and S. H. Bhavnani, "On the lateral fluid motion during pool boiling via preferentially located cavities," *Applied Physics Letters,* no. 104, 2014.

[9] SABIC IP , "ULTEM ™ Resin 1000," 2014. [Online]. Available: https://www.sabic-ip.com/gepapp/eng/weather/weatherhtml?sltRegionList=1002002000&sltPrd=1002003018&sltGrd=1002011252&sltUnit=0&sltModule=DATASHEETS&sltVersion=Internet&sltType=Online. [Accessed 2014].

[10] Omega Engineering, "GENERAL PURPOSE 100 MILLIVOLT OUTPUT PRESSURE SENSOR," 2003. [Online]. Available: http://www.omega.com/Pressure/pdf/PX302.pdf. [Accessed April 2014].

[11] Omega Engineering, "Thermocouples: An Introduction," [Online]. Available: http://www.omega.com/thermocouples.html. [Accessed April 2014].